Geol. Mag. **145** (*2*), *2008, pp. 215–233. © 2007 Cambridge University Press*
doi:10.1017/S0016756807004025 First published online 30 November 2007 *Printed in the United Kingdom*

Geochronology and geochemistry of Neoproterozoic mafic rocks from western Hunan, South China: implications for petrogenesis and post-orogenic extension

XIAO-LEI WANG*, JIN-CHENG ZHOU*†, JIAN-SHENG QIU*, SHAO-YONG JIANG* &YU-RUO SHI‡

*State Key Laboratory for Mineral Deposits Research, Department of Earth Sciences, Nanjing University, Nanjing 210093, PR China
‡Beijing SHRIMP Center, Chinese Academy of Geological Sciences, Beijing 100026, PR China

(*Received* 18 January 2007; *accepted* 1 May 2007)

Abstract – The Neoproterozoic mafic rocks in western Hunan, South China, form a NNE-striking mafic rock belt for which outcrops are found predominantly in Guzhang, Qianyang and Tongdao. Samples from Qianyang and Tongdao yielded ion microprobe U–Pb zircon ages of 747 ± 18 Ma and 772 ± 11 Ma, respectively. The mafic rocks are geochemically divided into two subtypes. Ultramafic rocks from Tongdao are depleted in Nb and Ti, with decoupled Nd–Hf isotopes, and geochemical features similar to the *c.* 761 Ma mafic–ultramafic rocks from Longsheng, northern Guangxi. Their $\varepsilon_{Nd}(t)$ value is −2.91, implying an enriched mantle source. Alkaline mafic rocks from Qianyang and Guzhang have high values of TiO_2, total alkali, some high field strength elements and $(La/Yb)_N$, and low Zr/Nb, La/Nb, Sm/Nd and $^{143}Nd/^{144}Nd$ ratios as well as coupled Nd–Hf isotopes. They are geochemically similar to ocean island basalts and show fractional crystallization of Fe–Ti oxides, olivine and pyroxene in the mafic magma. The *c.* 760 Ma mafic rocks in western Hunan may be the products of post-orogenic magmatism. After the Jinningian (Sibao) orogenic process, the upwelling of the deep asthenospheric mantle caused by the break-off and detachment of the subducted oceanic slab led to extension in the area. The extension might have taken place earlier in the Tongdao and Longsheng areas, which led to the partial melting of the lithospheric mantle that had been metasomatized during early oceanic subduction to generate a relatively large amount of sub-alkaline rocks. However, the less alkaline mafic rocks in Qianyang and Guzhang might have been generated in the relatively later stage of the extension, and may have resulted from a small degree of partial melting of the asthenospheric mantle.

Keywords: mafic rocks, petrogenesis, post-orogenic extension, Neoproterozoic, South China.

1. Introduction

The genesis of mafic rocks generated within orogenic belts remains the focus of considerable debate (Foden *et al.* 2002; Vilà *et al.* 2005). Post-orogenic mafic rocks are generally thought to be formed in extensional environments, such as post-orogenic extension (e.g. Teixeira *et al.* 2002; Zhou, M. F. *et al.* 2004), continental rifts (e.g. Coish & Sinton, 1992; Pedersen *et al.* 2002), etc. Distinguishing mafic magmatism formed in post-orogenic extension from that formed in other geodynamic settings is crucial for studying the evolution of orogenic belts.

The Proterozoic Jiangnan orogen is located between the Yangtze and Cathysia blocks (Fig. 1a). Igneous rocks in the orogen are dominated by Neoproterozoic S-type granitoids (Zhou, Wang & Qiu, 2005; Wang *et al.* 2006). Li *et al*. (2003) proposed that Neoproterozoic felsic and mafic magmatism in the Jiangnan orogen was related to the *c.* 840–740 Ma superplume activities that led to the break-up of the Rodinia supercontinent. However, compelling geological and petrological evidence for the hypothesis is lacking (Jiang, Sohl & Blick, 2003; Wang *et al.* 2004*a*; Zhou, J. C. *et al.* 2004). On the contrary, several lines of evidence seem to support the existence of a normal orogenic cycle for the Jiangnan orogen: (1) the *c.* 1000–950 Ma ophiolite suites (Chen *et al.* 1991; Zhou & Zhu, 1993; Li *et al.* 1994) and *c.* 910–875 Ma arc volcanic rocks (Cheng, 1993; Wang, 2000) in the eastern part of the Jiangnan orogen might record the early subduction of oceanic crust; (2) high-pressure blueschists with a K–Ar age of 866 ± 14 Ma probably indicate the collisional peak (Shu *et al.* 1994); and (3) it is proposed that the *c.* 835–800 Ma strongly peraluminous granitoids and mafic–ultramafic rocks in the western part of this orogenic belt would represent the post-collisional magmatism (Zhou, Wang & Qiu, 2005; Wang *et al.* 2004*b*, 2006). Thus, the 1000–800 Ma igneous rocks in the Jiangnan orogen may have resulted from the collision and the orogenesis between the Yangtze and Cathysia blocks. However, the geodynamic setting during *c.* 800–740 Ma for the

†Author for correspondence: j.c.zhou@public1.ptt.js.cn

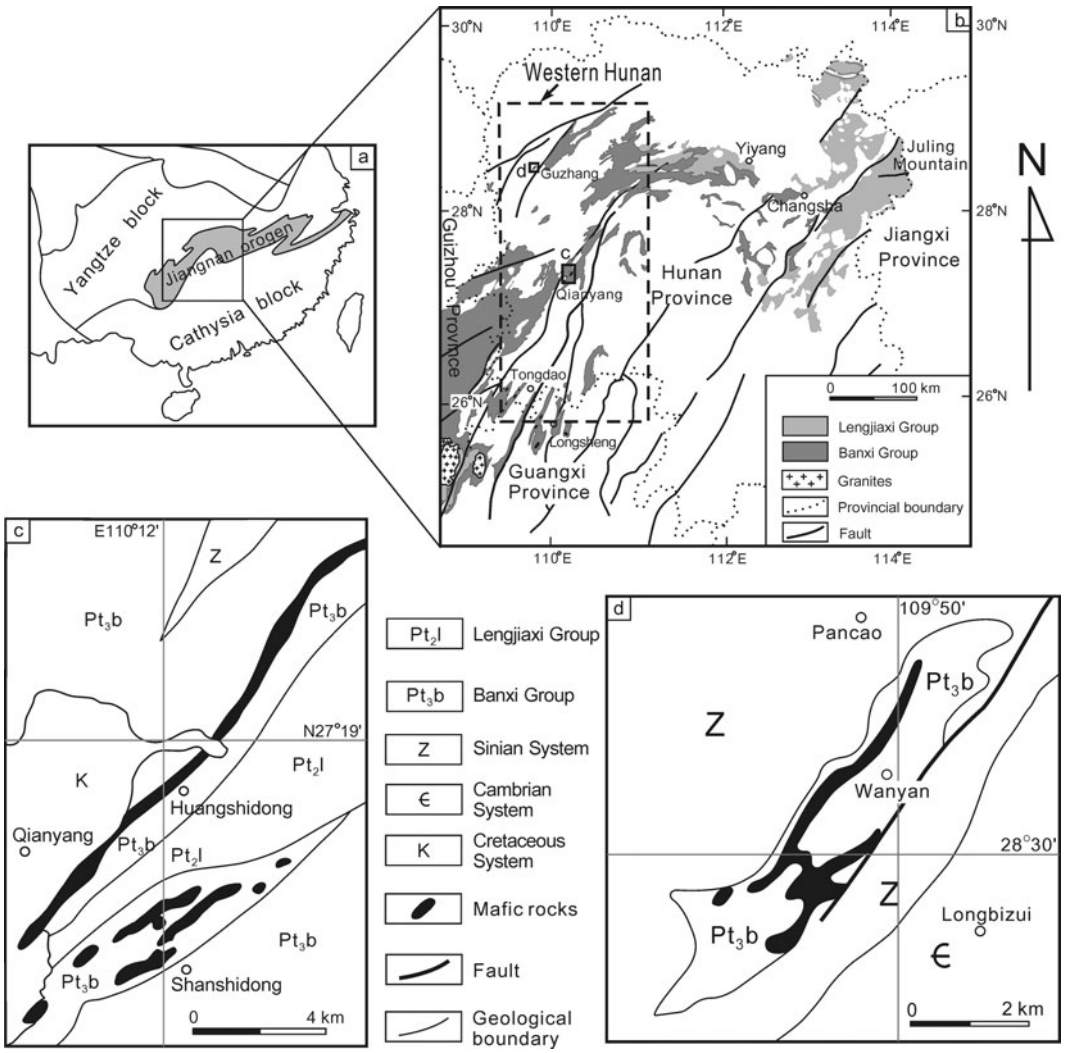

Figure 1. Geological sketch maps of western Hunan, South China (modified after HRGST, 1965; Zheng *et al.* 2001; Ma *et al.* 2002 and Wang *et al.* 2004*b*). (a) South China; (b) Hunan Provinces, with the dashed rectangle indicating the western Hunan area; (c) Qianyang; (d) Guzhang.

Jiangnan orogen is not clear. Recently, OIB (ocean island basalt)-like mafic rocks with ages of *c.* 760–750 Ma have been reported in the western Jiangnan orogen (Wang *et al.* 2004*b*; Zhou, Wang & Qiu, 2005). However, was the occurrence of these mafic rocks related to the alleged superplume activities? Also, it is still controversial whether South China was part of the Rodinia supercontinent during the period 800–740 Ma. In this work, we present new geochronological, element geochemical and Nd–Hf isotopic data for the mafic rocks in western Hunan. Their ages and petrogenesis will shed some light on the understanding of tectonic evolution of South China and some Neoproterozoic geological events.

2. Geological setting

The ENE-striking Jiangnan orogen is about 1500 km long and is situated on the southeastern margin of the Yangtze Block (Fig. 1a). The western part of the orogenic belt encompasses parts of northern Guangxi, western and northern Hunan, as well as northeastern Guizhou provinces (Fig. 1b). Two pre-Sinian sedimentary sequences, the Lengjiaxi and Banxi groups, occur in the area (Fig. 1b). They underwent low greenschist-facies metamorphism and are separated by an unconformity that is believed to mark the Jinningian orogenesis in the area (BGMRHN, 1988). Both sequences have been described in detail by Wang *et al*. (2004*b*). The Neoproterozoic Banxi Group constitutes the majority of the Precambrian sedimentary sequences in western Hunan. It is weakly deformed and is considered to be younger than *c.* 820 Ma (Wang & Li, 2003). The Banxi Group is subdivided into two formations. The lower Madiyi Formation comprises purple sandy conglomerates, arkose, pelitic dolomite and turbidite formed in a continental–neritic environment, whereas the upper Wuqiangxi Formation contains arkose, carbonaceous slate and marl deposited in a littoral–neritic environment. The two formations

exhibit characteristics of an extensional setting (Wang & Li, 2003). The Banxi Group is conformably overlain by the Lower Sinian System, which represents the deposits in a rift basin (Liu, Hao & Li, 1999). The Lower Sinian System, with age ranging from *c.* 750 Ma to 680 Ma, comprises the Chang'an, Xiangmeng and Nantuo formations from bottom to top in the area (Wang *et al.* 2004*b*; Wang & Li, 2003). In particular, it should be noted that the Chang'an and Nantuo formations in South China are considered to represent the Neoproterozoic Sturtian and Marinoan glacial deposits, respectively.

Neoproterozoic mafic magmatic rocks in western Hunan are mostly distributed in the Guzhang, Qianyang and Tongdao areas, constituting an approximately 300 km long NNE-trending rock belt (Fig. 1b), but their total outcrop area is less than 10 km^2 (BGMRHN, 1988). The NNE-trending belt may be extended southward to the Longsheng area of northern Guangxi (Fig. 1b). The mafic–ultramafic rocks in western Hunan occur predominantly as dykes, veins and sills. The intrusions are generally NNE-striking with individual widths of 10–200 m (BGMRHN, 1988). Most intrude the Wuqiangxi Formation and show conformable bedding planes with the country rocks (Fig. 1c, d; BGMRHN, 1988). Some diabases intersect the bedding of the country rocks. The contact zone between the mafic intrusions and the country rocks shows weak metamorphism, with contact metamorphic aureoles. There are a few basalts in the Wuqiangxi Formation near Qianyang city (Zheng *et al.* 2001). Mafic rocks in the Guzhang area are conformably overlain by the sandstones of the Lower Sinian System (Chang'an Formation; see Fig. 1d), suggesting their ages should be older than the lower age limit of the Sinian strata. According to their relationships with the overlying sedimentary sequences and their petrological features, the mafic–ultramafic rocks in western Hunan have been regarded as the products of a single episode of magmatism (BGMRHN, 1988; Zheng *et al.* 2001). However, their ages remain unknown. Zheng *et al.* (2001) obtained Sm–Nd whole-rock isochron ages of 868 ± 30 Ma and 855 ± 6 Ma for the basalts and pyroxenite-diabases, respectively, but both ages are questionable for their limited variation in Sm/Nd ratios. Recently, the ages of these mafic rocks from western Hunan have been estimated at 760–750 Ma based on new petrological and stratigraphic evidence in the adjacent areas (Wang *et al.* 2004*b*). Therefore, more precise geochronological studies are needed.

3. Petrography and mineralogy

Sampling was designed to cover the representative rock exposures in the southern (Tongdao area), middle (Qianyang area) and northern (Guzhang area) parts of western Hunan. Exposed rock types in the study area include altered pyroxenites, gabbros, gabbro-diabases, diabases and basalts. Gabbros and diabases are the dominant rock types (> 90 %) (BGMRHN, 1988). The mafic–ultramafic rocks from western Hunan generally experienced varying alteration and were replaced by tremolite, chlorite, clinozoisite, serpentine and calcite due to the low greenschist-facies metamorphism. Some relatively fresh clinopyroxene and plagioclase phenocrysts are observed in some mafic samples, but contents of the preserved clinopyroxenes and plagioclases vary in different samples. The accessory minerals within the mafic rocks are ilmenite and titanite.

Clinopyroxenes are subhedral to euhedral homogeneous augites with TiO_2 contents ranging from 0.40 wt % to 1.96 wt % (Table 1). The augites from Qianyang have higher TiO_2 and normative Wo than those from Guzhang, suggesting that the host basalts of the former have relatively high alkalis (Qiu & Zeng, 1987). Plagioclases are subhedral to euhedral, with normative Ab as high as 92.33 to 99.21. Albitization of the plagioclases is probably due to the regional low greenschist-facies metamorphism in the area.

4. Ion microprobe U–Pb zircon dating

4.a. Analytical techniques

Zircons for U–Pb analysis were separated from two samples (QY-2 and 05TD-3–3) by conventional magnetic and density techniques to concentrate non-magnetic, heavy fractions. About 3.0 kg from each sample was crushed. The zircons, together with several grains of TEMORA, were mounted in epoxy and polished down to half-section. Transmitted and reflected light micrographs and cathodoluminescence (CL) images were used to guide the U–Th–Pb isotope analyses, and the mount was vacuum-coated with a layer of high-purity gold. The CL study was carried out on a FEI-XL30SFEG electron microscope at the Department of Electronics, Beijing University. The zircon grains generally are 100–150 μm in length and 30–50 μm in width. CL images show typical rhythm zoning, indicating that the zircons are of magmatic origin. Zircon U–Pb isotopes were analysed by the Sensitive High-Resolution Ion MicroProbe (SHRIMP-II), the Beijing SHRIMP Centre, Chinese Academy of Geological Sciences. Detailed analysing processes are similar to Compston *et al.* (1992). A 3.2 nA primary beam, with about 30 μm diameter, was used for ion production. Five scans through the mass stations were made for each age determination. Both Pb/U and Pb/Th ratios and absolute Pb, Th and U abundances of the standard Sri Lanka zircon SL13 ($^{206}Pb/^{238}U = 0.0928$ corresponding to 572 Ma, 238 ppm ^{238}U: Williams, Buick & Cartwright, 1996) and TEM with an age of 417 Ma (Black *et al.* 2003) have been used to monitor the analyses of the zircon under study. ^{204}Pb was applied for the common lead correction and data processing

Table 1. Representative mineral compositions of clinopyroxenes (Py) and plagioclases (Pl) in the mafic rocks from western Hunan

Sample	QY-2		05GZ-15		05GZ-16		05GZ-19		05GZ-23		GZ-38	05GZ-15		05GZ-16	05GZ-19		05GZ-23
Mineral	Py	Py	Py	Py	Py	Py	Py	Py	Py	Py	Py	Pl	Pl	Pl	Pl	Pl	Pl
No.	1	2	3	4	5	6	7	8	9	10	11	12	13	14	15	16	17
Na_2O	0.31	0.34	0.24	0.27	0.34	0.47	0.26	0.34	0.26	0.26	0.27	10.01	10.20	10.46	9.85	11.14	9.61
K_2O	0.004	0.002	0.021	0.024	0.011	0.001	0.007	0.019	–	–	0.004	0.05	0.07	0.04	0.06	0.04	0.09
FeO	6.76	6.87	9.75	8.54	10.09	7.52	8.08	8.19	6.69	7.04	9.23	0.08	0.13	0.06	0.14	0.09	0.08
MgO	15.13	14.48	14.62	15.40	14.46	15.57	15.79	14.81	15.89	15.28	13.98	0.00	0.00	0.00	0.00	0.00	0.00
CaO	21.60	21.60	19.85	20.11	19.69	20.60	20.26	20.07	20.65	20.48	20.12	0.68	0.05	0.21	0.18	0.39	0.30
MnO	0.08	0.09	0.21	0.10	0.15	0.16	0.15	0.19	0.08	0.13	0.14	0.02	0.00	0.03	0.02	0.00	0.00
Al_2O_3	3.13	3.25	1.95	2.29	1.96	2.59	2.54	1.93	2.44	3.40	2.28	21.44	20.75	20.89	20.82	20.86	20.75
TiO_2	1.65	1.52	1.11	0.94	1.00	0.98	0.89	0.84	0.70	0.92	1.10	0.02	0.01	0.05	0.00	0.00	0.03
Cr_2O_3	0.22	0.30	–	0.07	0.07	0.24	0.23	0.11	0.42	0.60	–	–	–	0.03	0.06	–	0.07
SiO_2	50.98	50.97	51.46	51.76	51.88	51.85	51.98	53.29	52.33	50.95	53.30	68.32	68.83	69.48	69.33	67.68	69.01
Total	99.86	99.41	99.21	99.49	99.65	99.96	100.18	99.80	99.46	99.04	100.43	100.61	100.05	101.25	100.45	100.20	99.93
Mg no.	80	79	73	76	72	79	78	76	81	79	73						
En	43.9	42.8	42.5	44.5	42.2	45.0	45.3	43.8	46.1	45.0	41.6						
Fs	11.0	11.4	15.9	13.8	16.5	12.2	13.0	13.6	10.9	11.6	15.4						
Wo	45.1	45.9	41.5	41.7	41.3	42.8	41.7	42.6	43.0	43.4	43.0						
Na (Ab)	0.022	0.025	0.018	0.019	0.025	0.033	0.019	0.024	0.018	0.018	0.019	95.86	99.19	98.54	98.50	97.75	97.61
K (Or)	0.000	0.000	0.001	0.001	0.001	0.000	0.000	0.001	–	–	0.000	0.30	0.50	0.28	0.42	0.26	0.62
Fe (An)	0.210	0.214	0.306	0.266	0.316	0.233	0.250	0.253	0.207	0.219	0.285	3.84	0.31	1.18	1.08	1.99	1.77
Mg	0.835	0.803	0.819	0.856	0.806	0.859	0.869	0.816	0.876	0.849	0.768						
Ca	0.857	0.862	0.799	0.803	0.789	0.817	0.802	0.795	0.818	0.818	0.795						
Mn	0.003	0.003	0.007	0.003	0.005	0.005	0.005	0.006	0.003	0.004	0.004						
Al	0.137	0.142	0.087	0.100	0.086	0.113	0.111	0.084	0.106	0.149	0.099						
Ti	0.046	0.042	0.031	0.026	0.028	0.027	0.025	0.024	0.020	0.026	0.031						
Cr	0.007	0.009	–	0.002	0.002	0.007	0.007	0.003	0.012	0.018	–						
Si	1.889	1.897	1.934	1.928	1.941	1.918	1.920	1.970	1.935	1.899	1.964						

Mg no. = $100^{*}Mg^{2+}/(Mg^{2+}+Fe^{2+})$.

Table 2. Ion microprobe U–Th–Pb data for zircons from mafic rocks of Qianyang and Guzhang, western Hunan

Spot	% $^{206}Pb_C$	U (ppm)	Th (ppm)	Th/U	$^{206}Pb^*$ (ppm)	$^{206}Pb/^{238}U$	$\pm1\sigma$	$^{207}Pb/^{235}U$	$\pm1\sigma$	$^{207}Pb/^{206}Pb$	$(\pm1\sigma)$	$^{206}Pb/^{238}U$ age (Ma)	$(\pm1\sigma)$	$^{207}Pb/^{206}Pb$ age (Ma)	$(\pm1\sigma)$
Sample QY-2, Qianyang															
Q1.1	0.36	870	2941	3.38	93.1	0.1229	0.0054	1.085	0.066	0.06405	0.00237	747	31	743	80
Q2.1	0.49	656	2597	3.96	73.0	0.1251	0.0049	1.122	0.056	0.06503	0.00170	760	28	775	56
Q3.1	0.41	960	6094	6.34	108	0.1270	0.0065	1.182	0.068	0.06754	0.00130	771	38	854	40
Q4.1	0.36	1497	4611	3.08	169	0.1261	0.0073	1.117	0.068	0.06423	0.00087	766	42	749	29
Q5.1	0.39	1135	5077	4.47	121	0.1216	0.0065	1.053	0.061	0.06281	0.00101	740	37	702	35
Q6.1	1.61	746	2666	3.58	80.9	0.1203	0.0072	1.066	0.077	0.06426	0.00212	732	42	750	71
Q7.1	0.51	793	2717	3.43	85.3	0.1227	0.0062	1.086	0.063	0.06419	0.00144	746	36	748	48
Q8.1	0.30	1030	2945	2.86	111	0.1209	0.0063	1.109	0.063	0.06651	0.00105	736	36	823	33
Q9.1	1.64	1272	6145	4.83	140	0.1215	0.0065	1.162	0.072	0.06939	0.00169	739	38	910	51
Q10.1	0.80	643	3046	4.74	71.4	0.1248	0.0060	1.147	0.066	0.06669	0.00179	758	34	828	57
Q11.1	2.64	1304	4533	3.48	143	0.1195	0.0058	1.260	0.074	0.07649	0.00215	728	33	1108	57
Q12.1	2.40	1176	4949	4.21	127	0.1219	0.0066	1.192	0.109	0.07092	0.00480	742	38	955	145
Q14.1	0.37	1542	3931	2.55	164	0.1204	0.0056	1.121	0.058	0.06755	0.00117	733	32	855	36
Q15.1	0.44	623	2101	3.37	68.8	0.1240	0.0059	1.108	0.061	0.06484	0.00143	753	34	769	47
Sample TD-3–3, Tongdao															
T2.1	0.18	1679	4257	2.62	183	0.1267	0.0041	1.128	0.037	0.06457	0.00051	769	23	760	17
T3.1	0.64	256	750	3.03	28.8	0.1301	0.0043	1.202	0.053	0.06700	0.00188	788	25	839	59
T4.1	0.40	557	1486	2.76	61.3	0.1277	0.0042	1.147	0.041	0.06510	0.00104	775	24	778	33
T5.1	0.12	543	1210	2.30	56.1	0.1200	0.0040	1.086	0.038	0.06562	0.00079	731	22	794	26
T6.1	0.03	2483	4683	1.95	270	0.1267	0.0041	1.127	0.037	0.06450	0.00033	769	23	758	11
T7.1	0.20	540	1900	3.63	61.3	0.1318	0.0043	1.159	0.042	0.06375	0.00096	798	24	734	32
T8.1	0.21	457	1737	3.93	50.9	0.1294	0.0043	1.177	0.042	0.06593	0.00092	785	24	804	30
T9.1	0.11	361	1600	4.58	40.4	0.1304	0.0043	1.193	0.042	0.06636	0.00086	790	24	818	28
T10.1	0.06	747	2526	3.49	74.5	0.1160	0.0037	1.033	0.035	0.06459	0.00071	707	22	761	22
T11.1	0.13	1009	2912	2.98	109	0.1253	0.0040	1.112	0.038	0.06435	0.00060	761	23	753	20
T12.1	0.19	909	1846	2.10	97.0	0.1240	0.0040	1.108	0.038	0.06481	0.00071	754	23	768	24
T13.1	0.15	541	1195	2.28	58.2	0.1249	0.0041	1.133	0.040	0.06581	0.00079	759	24	800	24
T15.1	0.32	179	388	2.24	18.3	0.1190	0.0039	1.082	0.042	0.06600	0.00139	725	23	806	45
T16.1	0.35	450	1456	3.34	48.8	0.1257	0.0041	1.125	0.041	0.06490	0.00104	764	23	772	34
T17.1	0.13	481	1460	3.14	50.9	0.1230	0.0041	1.098	0.038	0.06477	0.00078	748	23	767	25
T19.1	0.05	1154	3633	3.25	114	0.1154	0.0037	1.041	0.034	0.06545	0.00052	704	22	789	17

Pb_C and Pb^* indicate the common and radiogenic lead proportions.

was carried out using the SQUID 1.0 (Ludwig, 1999) and PRAWN (Williams, Buick & Cartwright, 1996) programs. Uncertainties on individual analyses are quoted at the 1σ level, whereas those on pooled alignment analyses are quoted at the 95 % confidence level. Isotopic data are listed in Table 2.

4.b. Results

QY-2 is a diabase sampled from the Qianyang area. Fourteen spot analyses were performed on 14 zircon grains of the sample. The measured U and Th concentrations of these zircon grains range from 623 ppm to 1542 ppm and 2101 ppm to 2941 ppm, respectively. Th/U ratios are higher, varying between 2.55 and 6.34. Most of the analyses are concordant and yield a weighted mean ^{206}Pb–^{238}U age of 747 ± 18 Ma (Fig. 2a; 2σ, 95 % conf., $n = 14$, $MSWD = 0.14$). This age agrees with the weighted mean ^{207}Pb–^{206}Pb age of 776 ± 41 Ma of the sample (2σ, 95 % conf., $n = 12$, $MSWD = 1.7$) within analytical precision. For Neoproterozoic and younger rocks, the analysed zircon ^{206}Pb–^{238}U ages generally have higher precision than the ^{207}Pb–^{206}Pb ages (Black *et al.* 2003). The ^{206}Pb–^{238}U age of 747 ± 18 Ma is thus interpreted as the crystallization age of the Qianyang mafic rocks.

Sample 05TD-3–3 is from the Tongdao area, in the southern end of western Hunan. Sixteen analyses were obtained from 16 zircon grains from the sample. U and Th concentrations (179–2483 ppm and 388–4683 ppm, respectively) of the zircons have relatively wider ranges than those of QY-2. Th/U ratios are relatively high, ranging from 1.95 to 4.58. Common Pb is low, with a proportion generally less than 0.40 %, except for one analysis at 0.64 %. If all 16 analyses are treated as a single group they yield a weighted mean ^{206}Pb–^{238}U age of 756 ± 12 Ma (2σ, 95 % conf., $n = 16$, $MSWD = 1.6$). However, as shown in Figure 2b, some analyses are slightly discordant, which may result in a relatively young mean ^{206}Pb–^{238}U age. The $^{207}Pb/^{206}Pb$ ratios seem to be stable, giving a weighted average ^{207}Pb–^{206}Pb age of 772 ± 11 Ma (2σ, 95 % conf., $n = 16$, $MSWD = 0.9$). Considering the mean ^{207}Pb–^{206}Pb age has a relatively low MSWD value, we think 772 ± 11 Ma could represent the best estimate of the crystallization age of the Tongdao ultramafic rocks in these circumstances. This age is consistent with that of the Qianyang mafic rocks within analytical error.

5. Geochemistry

5.a. Analytical techniques

All samples were prepared by crushing in an agate shatterbox. Major elements were analysed using a VF-320 X-ray fluorescence spectrometer (XRF) at

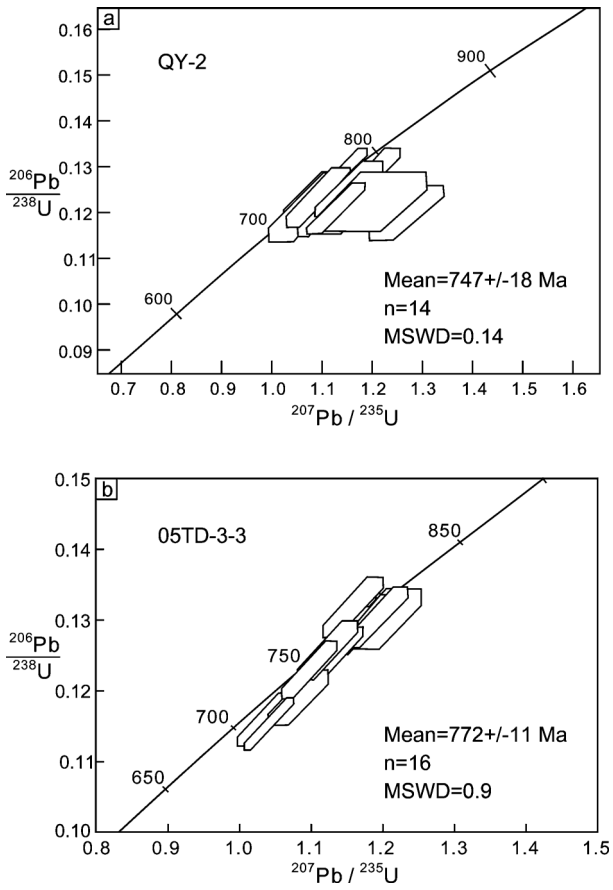

Figure 2. SHRIMP U–Pb zircon concordia plots and recalculated weighted mean $^{206}Pb/^{238}U$ ages for the Neoproterozoic mafic rocks from western Hunan. (a) QY-2, from Qianyang; (b) 05TD-3–3, from Tongdao.

the Centre of Modern Analysis, Nanjing University (NJU), with an analytical precision less than 1 %, following the procedures described by Franzini, Leoni & Saitta (1972). Rare earth elements (REE) and trace elements were determined by ICP-MS (Finnigan MAT Element 2) machines housed at the State Key Laboratory for Mineral Deposits Research, NJU. The analytical precision for most elements is better than 5 %. International standards were used to monitor the quality of analyses throughout the analytical processes for ICP-MS. Precisely weighed 50 mg sample powders were dissolved in Teflon bombs in $HF + HNO_3$. An internal standard solution containing the single element Rh was used to monitor signal drift during counting. Analytical procedures are similar those in Zhou, J. C. *et al*. (2004).

Sm–Nd isotopic compositions were determined at the Isotope Laboratory, Institute of Geology & Geophysics, Chinese Academy of Sciences (CAS), using a MAT-262 mass spectrograph. The analytical details have been given in Shen, Zhang & Liu (1997). Analysis of the standard BCR-1 gives $^{143}Nd/^{144}Nd = 0.512656 \pm 13$. The $\varepsilon_{Nd}(t)$ values were calculated based on the Nd isotopic compositions of $^{143}Nd/^{144}Nd$ (CHUR) $= 0.512638$ and $^{147}Sm/^{144}Nd$ (CHUR) $= 0.1967$.

Zircon Lu–Hf analyses reported here were carried out *in situ* using a Geolas CQ 193 nm ArF excimer laser ablation system at the Institute of Geology & Geophysics, CAS. The laser ablation system is attached to a Neptune MC-ICP-MS which has a double focusing multi-collector ICP-MS and the capability of high mass resolution measurements in a multiple collector mode. Both He and Ar carrier gases were used to transport the ablated sample from the laser-ablation cell via a mixing chamber to the ICP-MS torch. The analytical techniques are similar to those described in detail by Xu *et al*. (2004). Most analyses were carried out using a beam with an approximately 32 μm diameter and a 4 Hz repetition rate. A new TIMS determined value of 0.5887 for $^{176}Yb/^{172}Yb$ was applied for correction (Vervoort *et al.* 2004). During the analytical process, we applied the mean β_{Yb} value in the same spot to the interference correction of ^{176}Yb on ^{176}Hf in order to get precise data for the individual analyses. Zircon 91500 was used as the reference standard, with a recommended $^{176}Hf/^{177}Hf$ ratio of 0.282302 ± 8 (Goolaerts *et al.* 2004). The decay constant for ^{176}Lu of 1.865×10^{-11} a^{-1} proposed by Scherer, Münker, & Mezger (2001) was adopted in this work. ε_{Hf} values were calculated according to the chondritic values of Blichert-Toft, Chauvel & Albarede (1997).

5.b. Classification

Most of the rocks selected for this study are basalts and basaltic trachyandesites ($SiO_2 = 46.28$–57.47 wt %; Table 3; Fig. 3a, b). On the alkali–SiO_2 diagram (Fig. 3a), the samples from Qianyang and Guzhang are classified as basalts, trachybasalts and trachyandesites. Because the elements Ti, Zr, Nb and Y are not as susceptible to change during alteration as Na and K, a Zr/TiO_2–Nb/Y diagram (Winchester & Floyd, 1977) may be more reliable in distinguishing rock types than alkali–SiO_2 schemes. On such a diagram, the mafic rocks from Guzhang plot in the alkali basalt fields (Fig. 3b), while those from Qianyang are in the alkali basalts and trachyandesites areas. Both diagrams indicate that the samples from Qianyang and Guzhang are alkaline, whereas the samples from Tongdao plot in the sub-alkaline basalt area in both diagrams, similar to the mafic–ultramafic rocks from Longsheng, northern Guangxi (Fig. 3a, b). The rocks from Tongdao have high MgO (24.88–26.85 wt %), Ni (955–1237 ppm), Cr (1867–1975 ppm), Co (154–160 ppm) contents and low Na_2O, K_2O and P_2O_5 concentrations, indicating that they are ultramafic cumulates rich in normative enstatite and olivine.

5.c. Post-crystallization alteration

The mafic–ultramafic rocks collected for this study might undergo post-crystallization alteration and

Table 3. Major and trace element analyses for the Neoproterozoic mafic rocks from western Hunan, South China

No.	1	2	3	4[a]	5[a]	6[b]	7[b]	8[b]	9[b]	10	11[b]	12	13
				LS	LS								
				(n=17)	(n=3)								
Location[g]	TD	TD	TD	Average	Average	QY	QY	QY	QY	QY	QY	QY	QY
Sample	05TD-3-1	05TD-3-3	05TD-3-4		ultramafic	Qy-8	QY-1	Qy-2	Qy-3	QY-4	Qy-5	05QY-6	05QY-7
Rock type	Pyroxenite	Pyroxenite	Pyroxenite	mafic rocks	rocks	Basalt	Diabase	Diabase	Gabbro	Gabbro	Gabbro	Diabase	Diabase
SiO_2	47.11	46.37	46.28	51.80	43.43	45.82	48.47	50.18	53.73	52.31	54.23	47.67	49.91
TiO_2	0.56	0.61	0.58	1.10	0.75	2.56	2.01	1.85	2.96	3.46	2.34	1.70	3.39
Al_2O_3	7.66	7.34	6.91	14.99	7.17	13.90	13.88	12.91	15.09	18.86	14.76	12.72	17.68
Fe_2O_3	14.65[c]	15.25[c]	15.61[c]	2.17	1.89	2.34	3.38	2.84	1.42	2.58	2.00	14.47[c]	13.37[c]
FeO	–	–	–	7.82	12.58	9.10	9.82	8.86	9.53	8.06	9.17	–	–
MnO	0.25	0.26	0.29	0.15	0.22	0.18	0.19	0.19	0.20	0.10	0.17	0.19	0.18
MgO	24.88	25.96	26.85	9.64	28.31	10.76	12.11	11.72	3.71	3.64	2.63	13.36	3.83
CaO	4.72	4.00	3.21	7.25	4.12	11.11	5.58	6.60	5.50	2.21	5.74	5.93	4.38
Na_2O	0.00	0.00	0.00	3.22	0.00	1.95	3.11	3.32	6.08	8.03	6.27	2.73	5.88
K_2O	0.10	0.13	0.17	0.70	0.02	1.67	1.16	1.21	1.31	0.33	1.75	0.94	0.87
P_2O_5	0.08	0.09	0.09	0.16	0.10	0.61	0.29	0.33	0.48	0.41	0.94	0.29	0.51
LOI [d]	7.06	7.85	7.96	4.10	7.49	4.96	5.66	5.02	8.37	5.08	5.98	5.19	7.30
Mg no.[e]	77	77	77	62	78	63	63	65	38	38	30	65	36
Rb	4.01	10.40	15.05	18.72	2.48	20.18	24.85	22.45	15.82	6.62	35.75	51.02	22.07
Sr	15.10	24.34	20.88	196.4	33.05	1017	361.5	367.4	410.4	248.5	319.6	261.5	430.4
Ba	6.40	7.01	9.12	222.5	40.77	970.2	898.5	1059	387.2	137.7	610.3	430.4	424.9
Nb	2.80	3.12	3.82	5.06	2.55	53.98	21.31	25.81	38.24	33.95	48.69	25.58	40.57
Ta	0.30	0.29	0.51	0.47	0.23	3.77	1.29	1.80	2.73	2.08	3.36	1.87	2.77
Zr	68.76	71.80	76.61	112.4	53.80	306.9	185.3	209.2	266.9	251.1	399.0	215.3	331.7
Hf	1.77	1.84	2.14	2.86	1.42	6.93	3.99	4.89	6.11	5.43	8.74	6.52	8.12
Th	2.40	2.43	2.18	3.23	0.97	7.05	3.29	4.64	6.32	4.77	9.92	6.70	8.04
U	0.83	0.88	0.83	0.69	0.24	1.49	0.64	0.90	1.23	0.95	1.87	1.17	1.53
Cr	1975	1867	1895	457.3	2130	234.4	366.0	370.7	3.6	24.0	2.7	661.1	15.31
Ni	1237	1108	955	202.3	928.0	178.8	269.3	274.9	20.2	30.3	7.0	462.0	31.70
Sc	13.91	14.72	14.52	28.22	15.30	25.57	26.00	24.93	25.32	20.71	18.75	24.73	24.19
Pb	5.44	2.99	12.03	12.6	5.13	46.85	23.35	64.44	184.4	36.88	76.93	5.34	5.89
V	125.6	129.1	132.6	200.6	103.7	248.4	227.2	204.6	335.0	414.4	186.1	234.7	448.2
Co	154.4	159.9	157.7	50.92	115.5	51.60	65.90	59.80	28.11	26.11	24.26	94.39	45.16
La	6.81	7.09	7.45	11.45	4.10	56.04	28.11	27.15	41.09	39.12	63.58	31.49	41.62
Ce	12.05	14.09	13.20	25.30	9.63	106.1	62.02	48.71	80.19	80.59	121.83	49.59	76.96
Pr	1.60	1.61	1.64	3.71	1.36	11.70	5.95	6.01	9.26	7.89	13.72	5.63	9.72
Nd	8.00	8.46	7.25	14.85	5.88	45.79	23.00	25.06	36.35	28.42	57.08	26.06	43.45
Sm	2.03	2.36	2.38	3.73	1.44	9.14	4.68	5.45	8.06	6.28	11.97	5.80	8.83
Eu	0.38	0.44	0.57	1.08	0.28	2.67	1.42	1.68	2.23	1.75	3.09	1.57	2.24
Gd	2.02	2.12	1.88	3.97	1.53	8.04	5.52	5.24	7.45	6.82	11.02	4.34	6.45
Tb	0.41	0.42	0.30	0.66	0.28	1.08	0.71	0.74	1.03	0.99	1.56	0.69	0.96
Dy	2.63	2.58	1.85	3.99	1.64	5.91	3.96	4.32	6.16	5.54	9.06	3.93	5.87
Ho	0.62	0.62	0.41	0.81	0.32	0.96	0.72	0.75	1.06	1.04	1.54	0.78	1.19
Er	1.62	1.48	1.02	2.11	0.87	2.33	1.84	1.95	2.68	2.84	3.97	1.83	2.62
Tm	0.24	0.24	0.17	0.32	0.13	0.30	0.25	0.26	0.37	0.37	0.52	0.29	0.41
Yb	1.49	1.47	1.05	1.96	0.79	1.65	1.43	1.59	2.31	2.15	3.25	1.63	2.41
Lu	0.27	0.21	0.17	0.30	0.12	0.23	0.24	0.23	0.33	0.30	0.46	0.28	0.42
Y	17.36	15.40	12.45	22.12	9.79	23.73	12.63	18.21	26.56	19.09	37.23	19.49	29.22
Zr/Nb	24.56	23.01	20.05	21.78	20.49	5.69	8.69	8.11	6.98	7.40	8.19	8.42	8.18
Zr/Y	3.96	4.66	6.15	4.91	5.31	12.93	14.66	11.49	10.05	13.15	10.72	11.05	11.35
Nb/La	0.41	0.44	0.51	0.45	0.65	0.96	0.76	0.95	0.93	0.87	0.77	0.81	0.97
La/Ta	22.70	24.45	14.61	29.82	17.39	14.87	21.71	15.08	15.08	18.77	18.92	16.84	15.03
$(La/Yb)_N$	3.28	3.46	5.09	4.30	3.65	24.29	14.11	12.26	12.77	13.08	14.04	13.86	12.39
$(Gd/Yb)_N$	1.12	1.19	1.48	1.68	1.60	4.02	3.20	2.73	2.67	2.63	2.80	2.20	2.21

metamorphism in varying degrees, as indicated by their high LOI values (Table 3). This may disturb the abundance of individual elements. In this work, we put an emphasis on some elements, such as MgO, TiO_2, Al_2O_3, Ni, Cr, Y, high field strength elements (HFSEs) (Nb, Th, Ta, Zr and Hf) and REE (except Eu), which are relatively immobile during hydrothermal processes or low-grade metamorphism. To assess the mobility of individual elements during post-crystallization processes, we have plotted the less mobile MgO, Th, Y and La and the mobile Na_2O, K_2O, Sr and Ba elements against Zr (Fig. 4) which is relatively immobile (Winchester & Floyd, 1977; Macdonald *et al.* 1988). Plots of Na_2O, K_2O, Sr and Ba v. Zr for the rocks from Guzhang (Fig. 4) show a large scatter confirming their mobile nature, though some weak overall trends are observed. Plots of Th, Y and La v. Zr show correlations, suggesting that they might be immobile during post-crystallization alteration. Although a roughly negative correlation between MgO and Zr has been shown, there is still a mild scatter of data for the less mobile element. This is likely due to alteration effects. Both

Table 3. Continued.

No.	14	15	16	17	18	19	20	21	22	23	24[b]
Location[g]	QY	QY	QY	QY	GZ	GZ	GZ	GZ	GZ	GZ	GZ
Sample	05QY-8	05QY-9	05QY-11	05QY-13–2	05GZ-14	05GZ-15	05GZ-16	05GZ-19	05GZ-21–2	05GZ-23	GZ-38
Rock type	Gabbro	Gabbro	Gabbro-diabase	Gabbro-diabase	Diabase	Diabase	Diabase	Diabase	Diabase	Diabase	Diabase
SiO_2	57.47	56.74	55.55	55.28	50.48	51.31	51.13	49.05	51.78	48.99	51.75
TiO_2	1.59	1.86	2.29	2.93	1.49	1.86	1.61	2.12	1.69	1.72	1.83
Al_2O_3	17.49	16.92	17.08	18.86	14.60	15.32	15.80	15.18	15.02	14.57	15.29
Fe_2O_3	9.90[c]	10.89[c]	11.13[c]	10.44[c]	12.92[c]	12.90[c]	12.60[c]	13.95[c]	12.94[c]	14.24[c]	3.03
FeO	–	–	–	–	–	–	–	–	–	–	8.32
MnO	0.15	0.16	0.11	0.04	0.20	0.24	0.19	0.23	0.19	0.19	0.17
MgO	1.71	1.87	3.53	3.63	7.13	7.16	7.02	6.72	7.26	8.75	6.12
CaO	3.05	3.19	3.24	0.69	8.09	5.64	5.96	7.67	6.31	7.49	7.78
Na_2O	7.58	7.68	6.35	6.58	4.44	4.90	4.70	3.88	4.50	3.63	4.72
K_2O	0.57	0.10	0.25	1.09	0.39	0.41	0.78	0.92	0.12	0.23	0.72
P_2O_5	0.47	0.59	0.47	0.45	0.26	0.27	0.23	0.29	0.19	0.19	0.28
LOI[d]	8.21	4.63	4.57	2.71	3.67	3.21	3.38	2.80	7.77	7.38	3.60
Mg no.[e]	26	25	39	41	52	52	52	49	53	55	50
Rb	7.27	1.21	3.09	11.40	4.60	7.53	9.93	11.24	1.65	3.14	8.34
Sr	227.1	209.7	282.8	195.9	196.4	207.1	300.0	1058	598.2	632.5	556.2
Ba	145.0	57.89	166.6	554.8	232.3	320.9	404.4	530.9	165.7	296.1	400.6
Nb	60.55	60.92	34.68	38.05	16.33	20.80	17.66	26.06	15.59	14.02	19.94
Ta	4.00	4.25	2.40	2.63	1.15	1.41	1.22	1.71	1.07	1.47	1.47
Zr	574.2	536.3	344.3	315.6	178.8	252.3	211.9	248.3	154.0	148.3	165.7
Hf	15.60	15.33	8.33	8.05	4.59	6.06	4.76	5.87	3.94	3.84	4.29
Th	15.74	16.57	9.81	7.98	4.83	5.66	5.29	7.34	4.31	4.05	4.83
U	2.84	3.05	1.51	1.36	0.88	1.15	0.97	1.42	0.96	0.79	0.93
Cr	11.15	9.34	31.05	85.27	398.7	419.9	282.0	354.6	468.3	510.2	171.2
Ni	3.46	2.90	27.11	37.54	90.00	74.37	75.60	85.83	128.3	157.8	73.0
Sc	10.95	10.55	18.83	20.80	27.73	35.76	22.90	31.04	24.78	23.88	27.28
Pb	9.50	8.78	4.09	3.28	7.30	7.82	11.17	6.19	6.10	5.18	60.41
V	94.5	84.2	245.1	272.5	283.6	369.1	279.1	347.5	300.5	289.2	264.05
Co	13.07	17.64	30.67	24.38	56.30	53.80	52.58	61.88	59.06	62.22	44.73
La	70.51	78.76	46.82	38.27	23.25	32.38	26.25	33.16	19.24	20.48	26.16
Ce	107.4	131.1	76.94	64.48	44.87	55.37	46.42	57.39	37.12	34.51	46.00
Pr	13.75	15.64	9.25	8.22	4.76	6.44	5.04	6.53	4.31	4.25	5.88
Nd	55.03	65.89	40.59	37.98	23.10	27.60	23.68	30.09	20.22	18.57	24.41
Sm	12.75	13.70	9.45	7.65	5.54	6.62	5.73	7.12	4.90	4.68	5.49
Eu	2.96	3.37	2.29	1.90	1.28	1.67	1.58	1.81	1.47	1.55	1.62
Gd	8.04	9.70	6.14	4.92	3.91	4.99	4.11	4.95	3.71	3.52	5.19
Tb	1.43	1.53	0.87	0.78	0.70	0.80	0.67	0.79	0.60	0.57	0.76
Dy	7.91	9.00	5.16	4.73	3.72	4.19	3.78	4.68	3.17	3.14	4.51
Ho	1.62	1.76	1.11	0.99	0.75	0.97	0.79	0.97	0.74	0.68	0.78
Er	3.84	4.40	2.79	2.48	1.75	2.08	1.80	2.29	1.61	1.66	1.92
Tm	0.60	0.69	0.39	0.36	0.29	0.33	0.29	0.35	0.24	0.24	0.27
Yb	3.65	4.32	2.11	2.32	1.65	1.86	1.65	1.98	1.49	1.37	1.65
Lu	0.57	0.63	0.36	0.36	0.25	0.30	0.27	0.31	0.22	0.21	0.24
Y	38.55	40.19	27.53	25.89	17.49	23.77	19.06	23.98	15.74	15.63	18.41
Zr/Nb	9.48	8.80	9.93	8.29	10.95	12.13	12.00	9.53	9.88	10.58	8.31
Zr/Y	14.89	13.34	12.51	12.19	10.22	10.61	11.12	10.35	9.78	9.49	9.00
Nb/La	0.86	0.77	0.74	0.99	0.70	0.64	0.67	0.79	0.81	0.68	0.76
La/Ta	17.63	18.53	19.51	14.55	20.22	22.96	21.52	19.39	17.98	13.93	17.76
$(La/Yb)_N$	13.86	13.08	15.92	11.83	10.11	12.49	11.41	12.01	9.26	10.72	11.37
$(Gd/Yb)_N$	1.82	1.86	2.41	1.75	1.96	2.22	2.06	2.07	2.06	2.13	2.60

[a]Data sources: Ge *et al.* (2000) and Zhou J. C. *et al.* (2004); [b]data from Wang *et al.* (2004*b*), trace elements were re-analysed by ICP-MS; [c]Fe_2O_3 as total iron; [d]LOI, loss on ignition; [e]Mg no. $= 100*Mg^{2+}/(Mg^{2+}+Fe^{2+})$, Fe^{2+} is calculated from total Fe; [f]Major oxides were recalculated to 100% on a volatile-free basis; [g]TD – Tongdao, LS – Longsheng, QY – Qianyang.

the normalized REE and trace element patterns of the mafic rocks from western Hunan (Fig. 5) are generally regular, implying that most of the incompatible trace elements might be immobile during post-crystallization alteration and could be used to trace the magma sources.

5.d. Nature of parental magma

As shown in Table 3, mafic rocks from Qianyang and Guzhang show a range of compositions from fairly primitive (Mg no. = 65, Ni = 462 ppm, Cr = 661 ppm) to highly differentiated (Mg no. = 25, Ni = 2.9 ppm, Cr = 2.68 ppm). It is therefore important in later discussion of mantle source characters to choose element ratios that are not significantly affected by crystal fractionation processes. These rocks have high TiO_2, moderate Al_2O_3 contents and low Al_2O_3/TiO_2 ratios. Total alkalis are relatively high (3.62–8.36 wt %). LREE (light rare earth elements) are highly enriched relative to HREE (heavy rare earth elements) (Fig. 5;

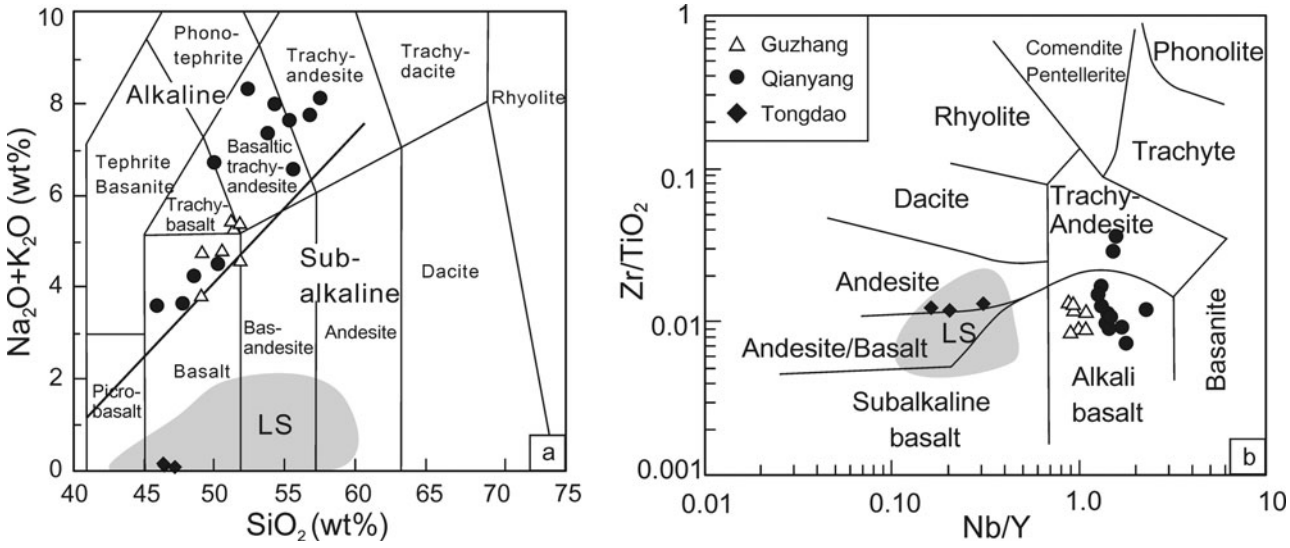

Figure 3. Rock classification diagrams for the Neoproterozoic mafic rocks from western Hunan. (a) TAS diagram (after Maitre *et al.* 1989); (b) Zr/TiO_2–Nb/Y diagram (after Winchester & Floyd, 1977). The shaded areas outline the ranges of compositions for the mafic–ultramafic rocks from the Longsheng area of northern Guangxi with data sources from Zhou, J. C. *et al.* (2004) and Ge *et al.* (2000).

$(La/Yb)_N = 9.26–25.29$, $(Gd/Yb)_N = 1.75–3.85$). The samples from Qianyang, with higher TiO_2, P_2O_5 and Zr contents and Nb/Y ratios (Table 3; Fig. 3b), are more alkaline than those from Guzhang. The Qianyang mafic rocks also have higher LREE contents (average La concentrations of 46.13 ppm for Qianyang as opposed to 26.04 ppm for Guzhang samples) and fractionated REE patterns ($(La/Yb)_N$ values of 11.83–25.29 v. 9.26–12.49). There is an overall similarity in the trace element patterns for the mafic rocks from Qianyang and Guzhang, and most of them are enriched in incompatible elements (Fig. 5). The HFSE, such as Nb, Zr, Hf and Ti, are generally not depleted. Although the rocks show a slight Nb depletion relative to U and La, they do not show extreme Nb depletion like the island arc basalts (Kelemen *et al.* 1990). Zr and Hf are even enriched in some samples. The variations in Rb and Ba might result from the post-crystallization alteration.

Overall, the primitive-mantle normalized patterns of the mafic rocks from Qianyang and Guzhang are regular and similar to those of typical ocean island basalts (OIB). Incompatible trace element ratios, such as Zr/Nb (6.15–12.15) and La/Nb (0.96–1.56, average of 1.26), are also similar to EM-1 type OIB (Weaver, 1991). Their low Rb/Sr and Sm/Nd ratios (0.02–0.13 and 0.19–0.22, respectively) as well as lower $^{143}Nd/^{144}Nd$ ratios (between 0.51228 and 0.51237, Table 4) and initial ($^{87}Sr/^{86}Sr$) ratios (Wang *et al.* 2004b), are similar to those of the EM-1 type OIB in Walvis Ridge (Saunders & Tarney, 1988). The $\varepsilon_{Nd}(t)$ values of these alkaline mafic rocks range from −0.47 to 2.69 (Table 4), suggesting that they might be derived from a weakly depleted mantle source. Moreover, it is evident that most $\varepsilon_{Nd}(t)$ values of the mafic intrusive rocks from Qianyang and Guzhang are near chondritic (−0.47 to 0.93) except for one basalt sample (QY-8). This

Table 4. Sm–Nd isotopic data for the Neoproterozoic mafic rocks from western Hunan, South China

No.	Sample	Age (Ma)	Sm (ppm)	Nd (ppm)	$^{147}Sm/^{144}Nd$	$^{143}Nd/^{144}Nd$	$\pm2\sigma(10^{-6})$	$\varepsilon_{Nd}(T)$	T_{DM} (Ma)
1	05TD-3-3	760	2.024	6.724	0.1822	0.512417	18	−2.91	1676
2[a]	QY-2	760	5.057	23.93	0.1278	0.512338	8	0.85	1372
3[a]	QY-3	760	6.318	29.55	0.1293	0.512316	10	0.27	1419
4[a]	QY-5	760	9.995	47.48	0.1273	0.512311	15	0.37	1411
5	05QY-7	760	8.612	41.65	0.1252	0.512320	13	0.75	1380
6[a]	QY-8	760	8.287	43.68	0.1148	0.512370	11	2.74	1219
7	05QY-9	760	11.83	57.98	0.1235	0.512282	13	0.17	1427
8	05QY-11	760	8.323	40.70	0.1238	0.512287	12	0.24	1422
9	05QY-13-2	760	7.619	37.08	0.1244	0.512296	13	0.36	1412
10	05GZ-14	760	5.343	23.93	0.1351	0.512323	14	−0.16	1454
13	05GZ-15	760	5.910	26.81	0.1335	0.512323	12	0.00	1441
14	05GZ-16	760	5.242	23.96	0.1324	0.512303	11	−0.29	1464
15	05GZ-19	760	6.218	28.82	0.1306	0.512309	13	0.01	1440
16	05GZ-23	760	4.527	20.14	0.1361	0.512314	14	−0.43	1476
17[a]	GZ-38	760	4.953	22.91	0.1307	0.512359	11	0.97	1362

[a]Data from Wang *et al.* (2004*b*)

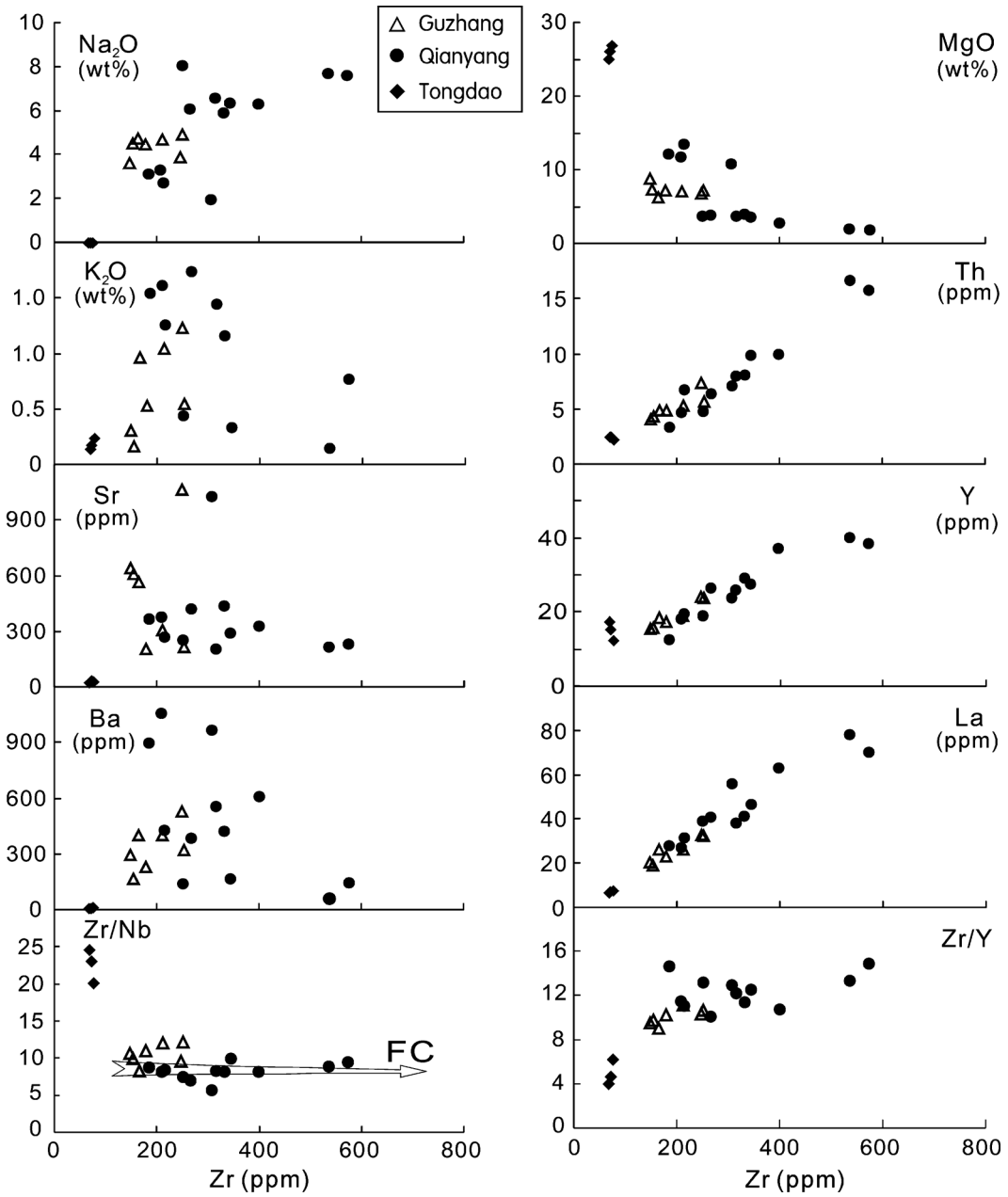

Figure 4. Major, trace elements and incompatible element ratios v. Zr for the Neoproterozoic mafic–ultramafic rocks from western Hunan. FC – fractional crystallization.

suggests the involvement of some enriched components in their sources.

The Tongdao ultramafic rocks as well as the mafic–ultramafic rocks from Longsheng of northern Guangxi show clearly different geochemical characteristics. They generally have low TiO_2, Na_2O, K_2O and P_2O_5 and are enriched in MgO, MnO, Ni and Cr (Table 3). The enrichment of LREE for the Tongdao ultramafic rocks is relatively low, with average $(La/Yb)_N$ of 3.94 (Fig. 5), similar to those of the mafic–ultramafic rocks from Longsheng. The REE patterns of these rocks show moderate negative Eu anomalies ($Eu/Eu* = 0.57$–0.80), implying the fractionation of plagioclase. The evident Sr troughs in the primitive-normalized patterns also support this conclusion (Fig. 5). There are moderate to weak negative anomalies in Nb and Ti, but Zr and Hf are not depleted. Compared to the mafic rocks from Qianyang and Guzhang, the Tongdao ultramafic rocks have high $^{147}Sm/^{144}Nd$ and $^{143}Nd/^{144}Nd$ values with a $\varepsilon_{Nd}(t)$ value of -2.91 (Table 4), implying the enriched signatures in their source.

5.e. Zircon Hf isotopes

Since zircon preserves a high-quality record of near-initial Hf-isotope ratios, it can be utilized as a geochemical tracer of a host rock's origin (Woodhead *et al.* 2004). The dated zircons of this work were

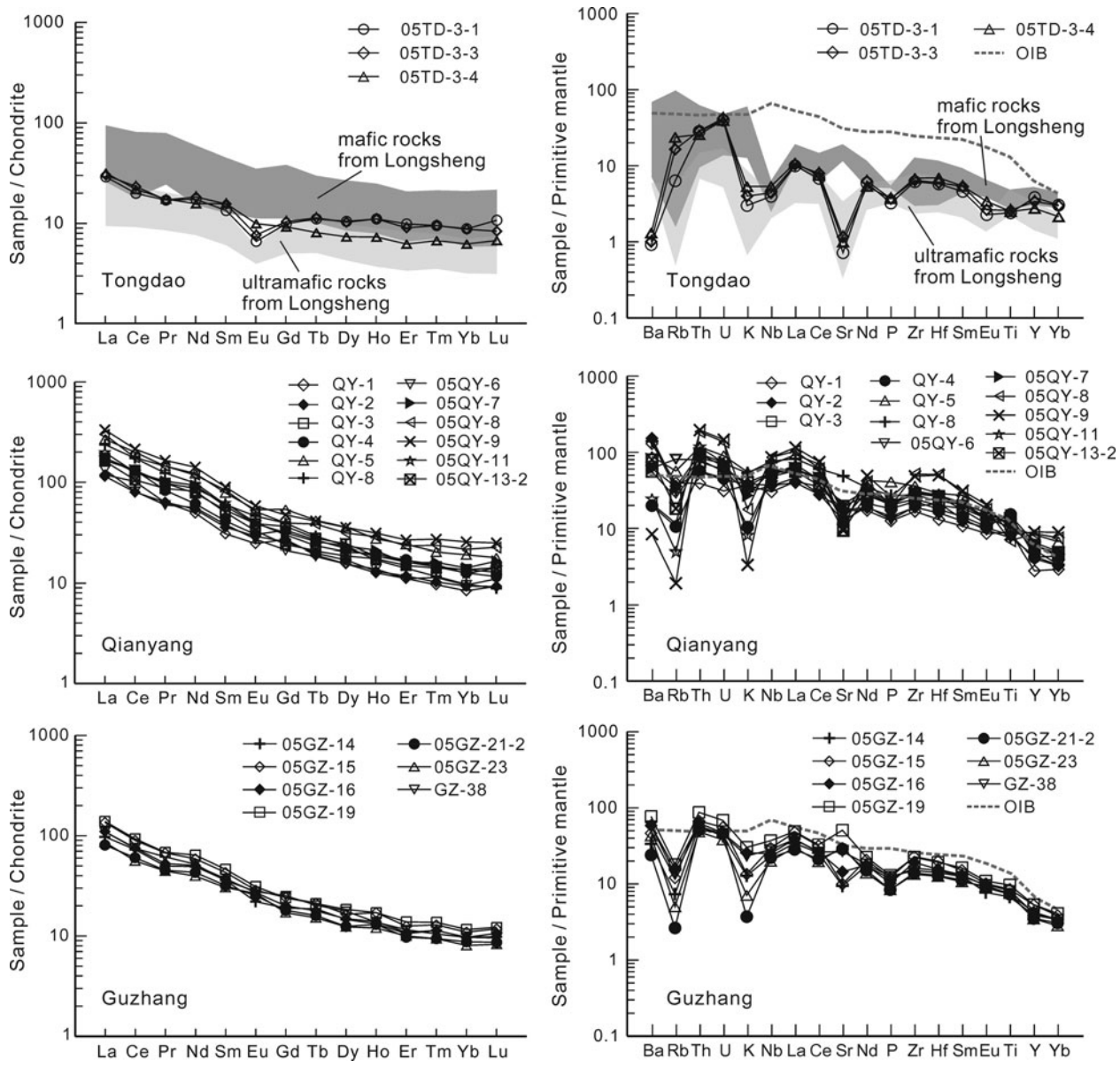

Figure 5. Normalized REE and trace element patterns for the Neoproterozoic mafic rocks from western Hunan. Chondrite, primitive mantle and OIB data are from Sun & McDonough (1989).

further analysed for micro-area Lu–Hf isotopes and the results are listed in Table 5 (supplementary material, available online at the *Geological Magazine* website http://journals.cambridge.org/geo). Initial $^{176}Hf/^{177}Hf$ ratios were calculated using their determined U–Pb zircon ages. We determined the Lu–Hf isotopic compositions of 18 and 17 spots for samples QY-2 and 05TD-3–3, respectively. As shown in Figure 6, the weighted average initial $^{176}Hf/^{177}Hf$ ratios of the zircons from QY-2 are basically similar to those from 05TD-3–3. The zircon $\varepsilon_{Hf}(t)$ values of QY-2 vary from −1.96 to +8.50, while the $\varepsilon_{Hf}(t)$ values of 05TD-3–3 range from −0.86 to +5.65. Although the $^{176}Hf/^{177}Hf$ ratios of the two samples display multi-peak distributions (Fig. 6), they are generally restricted to a range of 0.2823–0.2825. Therefore, we think the weighted mean values of the Hf isotopes and the corresponding $\varepsilon_{Hf}(t)$ values (Fig. 6; 1.0 ± 1.1 for QY-2 and 1.91 ± 0.95 for 05TD-3–3, respectively) could approximately represent the initial Hf isotopic compositions of the two samples. The average $\varepsilon_{Hf}(t)$ value of QY-2 (1.0 ± 1.1), consistent with its $\varepsilon_{Nd}(t)$ value (0.85, Table 4), is near chondritic. It indicates that the Nd–Hf isotopes of mafic rocks from Qianyang and Guzhang are coupled with each other. In the ultramafic rocks from Tongdao, however, the $\varepsilon_{Nd}(t)$ value of 05TD-3–3 (−2.91, Table 4) is evidently decoupled from its $\varepsilon_{Hf}(t)$ value (1.91 ± 0.95).

6. Magma genesis

6.a. Crustal contamination

Mantle-derived magmas may be affected by crustal contamination during their ascent, and/or temporary

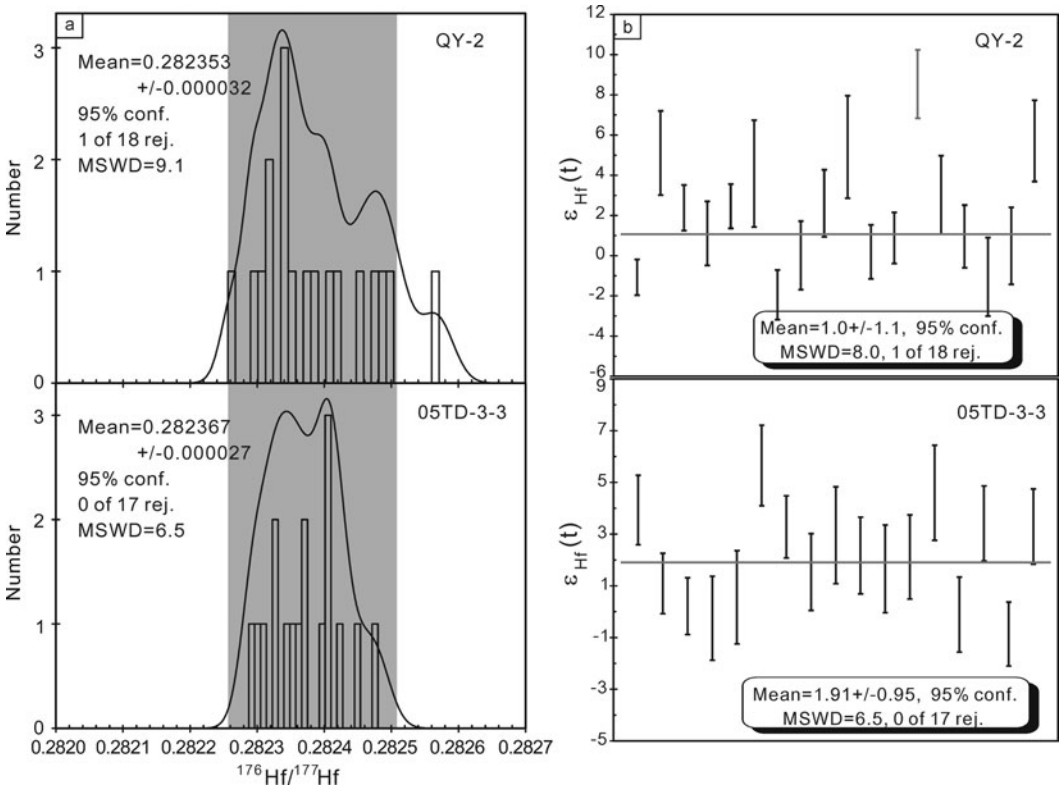

Figure 6. Hf isotopes and the recalculated weighted average $\varepsilon_{Hf}(t)$ values for the Neoproterozoic mafic rocks from western Hunan. QY-2, from Qianyang; 05TD-3–3, from Tongdao. The shaded area is used for comparison.

residence in magma chambers within continental crust. Some samples (QY-3, 4, 5, 7, 8) have normative nepheline (Table 3), which does not support the significant high-SiO_2 crustal component assimilation. In addition, there are no positive correlations between La/Sm v. Zr/Nb, La/Sm and La/Nb v. $^{143}Nd/^{144}Nd$, and negative correlation of Ti/Zr v. La/Nb for the mafic rocks from Qianyang and Guzhang, implying that the crustal contamination was not an important factor for the generation of these Neoproterozoic mafic rocks.

6.b. Fractional crystallization

The mafic rocks from Qianyang and Guzhang have Mg no. ranging from 65 to 25, suggesting that fractional crystallization is an important factor in the evolution of the mafic magmas in the area. Moreover, the Zr/Nb–Zr plot (Fig. 4) implies that the slight chemical differences between samples would reflect variations in the degree of fractional crystallization rather than partial melting. The effects of fractional crystallization for the mafic rocks from western Hunan are indicated by the compositional variations of both major and trace elements with respect to Mg no. as fractionation index (Fig. 7). CaO, CaO/Al_2O_3 and CaO/TiO_2 increase with the increased Mg no. (Fig. 7), which indicates the crystallization of clinopyroxene (Class *et al.* 1994). It should be pointed out that two types of correlations with Mg no. have been shown by some elements and element ratios (Fig. 7). Under Mg no. ≥ 45 (predominantly including the ultramafic and mafic rocks), negative correlations are revealed by TiO_2, Al_2O_3, Na_2O+K_2O and V versus Mg no., whereas positive correlations exist between Al_2O_3/TiO_2 and Mg no., implying the fractional crystallizations of olivine and clinopyroxene. Under Mg no. < 45, however, there are positive correlations of TiO_2 and V versus Mg no., relatively constant $Na_2O + K_2O$ and Al_2O_3 versus Mg no., and negative correlation of Al_2O_3/TiO_2 versus Mg no., probably indicating the fractionation of Fe–Ti oxides. Incompatible trace elements (e.g. Zr, Nb and Y) show negative correlations with Mg no., while the compatible trace elements (e.g. Ni and Cr) have positive correlations with Mg no., supporting the fractionation of olivine and pyroxene. Furthermore, a Eu anomaly is lacking in most mafic samples (Fig. 5), indicating that plagioclase fractionation was not important in the mafic magma evolution.

6.c. Magma source

Although the mafic rocks from Tongdao, Qianyang and Guzhang occur in the same magmatic belt, the elemental geochemical and Sm–Nd isotopic features discussed above suggest that these contemporaneous rocks may have been derived from rather different mantle sources.

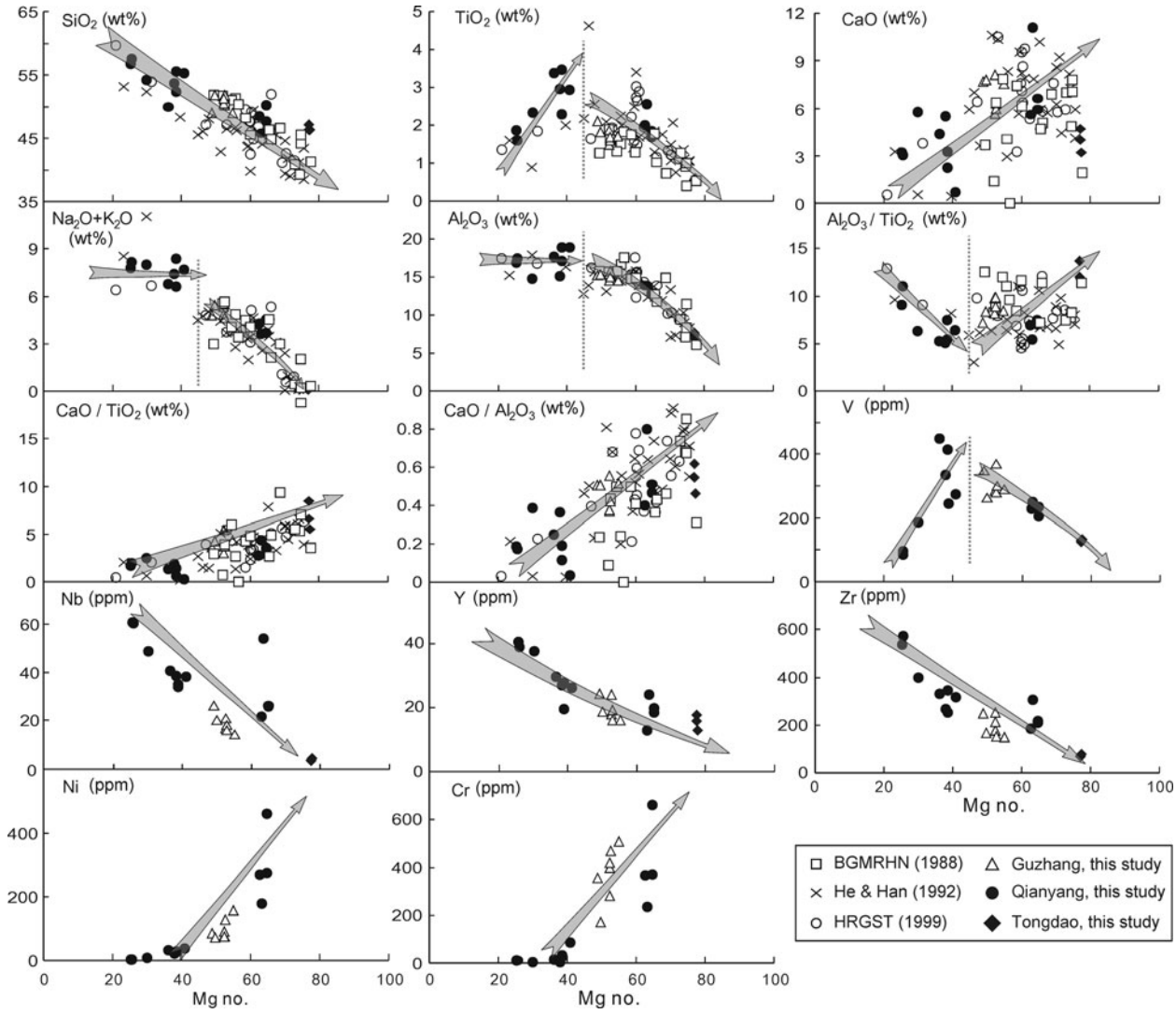

Figure 7. Major and trace elements v. Mg no. plot for the Neoproterozoic mafic rocks from western Hunan.

6.c.1. Tongdao

As shown in Figure 1b, the Neoproterozoic mafic rock belt in western Hunan extends southward to the Longsheng area of northern Guangxi Province. The mafic rocks from Longsheng yielded a single zircon U–Pb age of 761 ± 8 Ma (Ge *et al.* 2001), which is indistinguishable from that of the Tongdao rocks (772 ± 11 Ma). It is therefore necessary to bring together different studies of the mafic–ultramafic rocks from both Tongdao and Longsheng in order to discuss their petrogenesis. The mafic–ultramafic rocks from Longsheng have been believed to be derived from lithospheric mantle (Ge *et al.* 2000; Zhou, J. C. *et al.* 2004). The ultramafic rocks from Tongdao show obvious geochemical affinities with those from Longsheng, implying a petrogenetic correlation between them. In tectonic discriminant diagrams (Fig. 8), the ultramafic rocks from Tongdao all plot in the volcanic arc basalt area, similar to those from Longsheng.

The decoupled Nd–Hf isotopic compositions of the Tongdao ultramafic rocks are likely to reflect the influence of an early subduction process in their mantle source. In the subduction zone, the addition of subducted components would increase Nd more than Hf concentrations in the mantle wedge. This is because Nd is more soluble than Hf in slab-derived fluids and melts that have typically high Nd/Hf ratios (Polat & Münker, 2004). In the Baotan area of northern Guangxi, about 140 km southwest of the Longsheng area, the occurrence of the Mesoproterozoic and *c.* 820 Ma mafic–ultramafic rocks is believed to be related to the early subduction and post-collisional processes in the area (Zhou, J. C. *et al.* 2004; Wang *et al.* 2006). The *c.* 760 Ma mafic magmatism from Tongdao in western Hunan and Longsheng in northern Guangxi clearly took place following the orogenic process. Their mantle source might have been metasomatized by the early slab-derived components in the area. Overall, the decoupled Nd–Hf isotopic characteristics

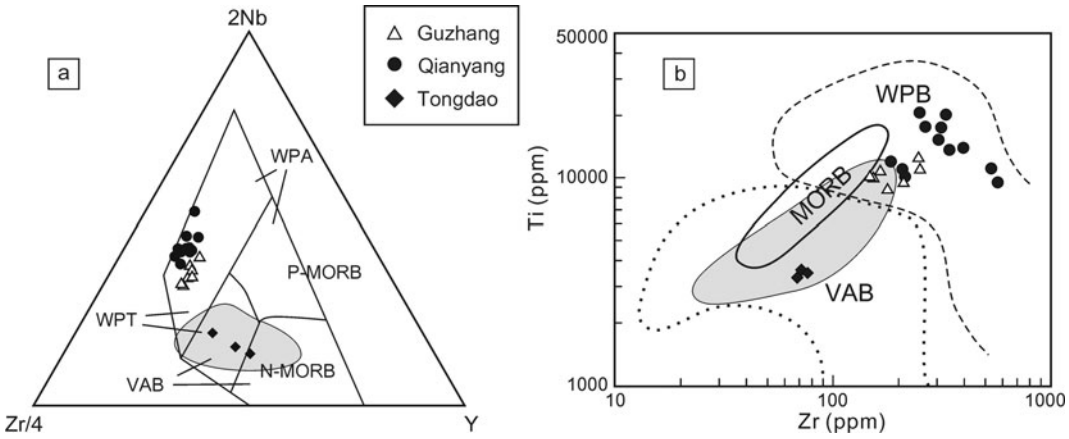

Figure 8. Tectonic discriminative diagrams for the Neoproterozoic mafic rocks from western Hunan. (a) 2Nb–Zr/4–Y plot (after Meschede, 1986); (b) Ti–Zr plot (after Pearce, 1982). WPA – within-plate alkaline basalts; WPB – within-plate basalts; WPT – within-plate tholeiites; VAB – volcanic arc basalts; MORB – middle ocean ridge basalts; N-MORB – normal MORB; P-MORB – plume MORB. The shaded areas outline the ranges of compositions for the mafic–ultramafic rocks from the Longsheng area with data sources from Zhou, J. C. *et al.* (2004) and Ge *et al.* (2000).

of the Tongdao ultramafic rocks provide another line of important evidence for the origination of these rocks from the partial melting of early metasomatized lithospheric mantle.

6.c.2. Qianyang and Guzhang

The mafic rocks from Qianyang and Guzhang are characterized by their high alkali and TiO_2 contents and OIB-like trace element patterns. They consistently plot in the within-plate basalt area in tectonic discriminant diagrams (Fig. 8). The origin of the within-plate mafic rocks is still the subject of debate. They can be generated by the melting of the continental lithospheric mantle, the asthenospheric mantle or both (McDonough, 1990; McKenzie & O'Nions, 1995). Most authors believe that they might be derived from a relatively enriched mantle source (e.g. Halliday *et al.* 1995; Lassiter *et al.* 2003). During continental extension under very high stretching factors ($\beta = 3.5$–6), lithosphere which has been previously enriched by CO_2–H_2O-rich metasomatic fluids derived from the asthenosphere could be partially melted to generate the OIB-like magmas (McKenzie & Bickle, 1988; Arndt & Christensen, 1992). However, there is no evidence for significantly stretched lithosphere in the western part of the Proterozoic Jiangnan orogen. Therefore, a lithospheric mantle source for the alkaline mafic magmas from Qianyang and Guzhang of western Hunan is less likely. These alkaline mafic rocks are geochemically similar to the OIB and comparable to the alkali basalts from the Basin and Range Province of the western U.S.A. (Bradshaw, Hawkesworth & Gallagher, 1993). This indicates that an asthenospheric mantle source might be suitable for them.

In addition, it has been reported that some geochemical criteria could be used to distinguish the asthenospheric and lithospheric mantle-derived basalts. Thompson & Morrison (1988) showed that basaltic rocks with La/Ta ratios of 10–12 might be derived from the asthenospheric mantle, whereas basalts having La/Ta > 30 were derived from the lithospheric mantle or had suffered crustal contamination. Fitton *et al.* (1988) and Saunders *et al.* (1992) also used La/Nb ratios to distinguish the basalts derived from different mantle sources. They found that the basalts derived from uncontaminated asthenospheric mantle have La/Nb ratios of < 1.5, while those from a lithospheric mantle have a La/Nb > 1.5. In the Neoproterozoic alkaline mafic rocks from Qianyang and Guzhang, La/Ta ratios range from 13.01 to 22.96 (average 17.11) and La/Nb ratios vary from 0.96 to 1.56 (average 1.26). It suggests that their parental magmas have been derived from the asthenospheric mantle.

Moreover, the $\varepsilon_{Nd}(t)$ values of the intrusive rocks from Qianyang and Guzhang are near chondritic (between −0.43 and 0.97; Table 4) except for a basalt sample (QY-8), as pointed out above. Similarly, the mean $\varepsilon_{Hf}(t)$ value of zircon grains in QY-2 is also near chondritic (1.0 ± 1.1). The coupled Nd–Hf isotopic compositions of these rocks might provide some useful information for their petrogenesis. During the earlier extension stage immediately following the orogeny, some older enriched lithospheric mantle components might be incorporated into the depleted asthenospheric mantle. The mixing between the incorporated enriched lithospheric mantle and the depleted mantle would cause the mantle source to have near-chondritic Sm–Nd and Lu–Hf isotopic signatures. Therefore, essentially near-chondritic $\varepsilon_{Nd}(t)$ and $\varepsilon_{Hf}(t)$ values for the mafic intrusive rocks from Qianyang and Guzhang likely reflect the interactions between the depleted asthenospheric and enriched lithospheric mantle along the Jiangnan orogen during Neoproterozoic times.

7. Tectono-magmatic evolution model

In recent years, much discussion has focused on the Precambrian tectonic evolution of South China (e.g. Zhao & Cawood, 1999; Li *et al.* 1999, 2003; Zhou *et al.* 2002; Yang *et al.* 2004). It is generally accepted that the Jiangnan orogen resulted from the collision between the Yangtze and Cathysia blocks (Guo, Shi & Ma, 1980; Chen *et al.* 1991; Zhou & Zhu, 1993; Zhao & Cawood, 1999; Wu, Zheng & Wu, 2005). Corresponding petrological records include the 1.0–0.96 Ga ophiolites, the *c.* 910–875 Ma arc volcanic rocks, the high-pressure blueschists of 870–850 Ma and the post-collisional S-type granitic rocks emplaced at 835–800 Ma. There was no magmatism during 790–770 Ma in the western part of the Jiangnan orogen, which might suggest a transition of tectonic regime in the area. The occurrence of *c.* 760 Ma mafic–ultramafic rocks in western Hunan as well as those in Longsheng of northern Guangxi may be the products of post-orogenic magmatism.

There are two possible explanations for the *c.* 760 Ma mafic magmatism of the western Jiangnan orogen. The first explanation involves a (super-)mantle plume event (Li *et al.* 1999, 2003), whereas the second one can be viewed in a model of post-orogenic extension that follows continental collision.

The mantle plume model encounters significant difficulties in explaining the origin of the Neoproterozoic mafic rocks in the western Jiangnan orogen. First, a considerable lack of outcrop of large-scale mafic lavas and dykes seems to conflict with the (super-)plume model. There is only about 100 km^2 of outcropping area for the *c.* 760 Ma mafic rocks in the western part of the Jiangnan orogen (including western Hunan and northern Guangxi: BGMRHN, 1988; BGMRGX, 1985). Second, the aeromagnetic anomaly resulting from mafic rocks in the area is very weak (Rao, Wang & Cao, 1993), which suggests that the amount of mafic rocks exposed and buried in the area is limited. Third, high-magnesium and high-alkali mafic–ultramafic rocks are absent in the area.

Post-orogenic extension might be considered as an alternative model for the geodynamic setting of the *c.* 760 Ma magmatism in the western part of the Jiangnan orogen. Bonin *et al*. (1998) have given definitions for the different episodes of a whole orogenic Wilson cycle, and proposed that the post-orogenic episode would be likely to occur after the orogenic processes and during the within-plate stage. Delamination of the subcontinental lithosphere (Wu *et al.* 2004), upwelling of new asthenospheric mantle, thinning of overlying lithospheric mantle (Zhou, M. F. *et al.* 2004) and collapse of the orogenic belt (England & Houseman, 1989) would lead to the extension in the post-orogenic stage. The NNE distribution style of the *c.* 760 Ma mafic magmatism in the western part of the Jiangnan orogen (Fig. 1a) is consistent with the strike of the pre-existing subduction zone in the area. It is believed that the pre-existing metasomatized lithospheric mantle would be easily melted during the post-orogenic extension. Therefore, for the petrogenesis (see discussion below) of the *c.* 760 Ma mafic rocks in the western Jiangnan orogen, the post-orogenic extension model would also be preferred.

It is well known that the coexistence of nearly coeval mafic magmas derived from different sources like this is common in orogenic belts worldwide (Dunphy, Ludden, & Francis, 1995; Foden *et al.* 2002; Cvetković *et al.* 2004). It has been noted that the mafic rocks from Qianyang and Guzhang derived from asthenospheric mantle have only an area of less than 10 km^2 (BGMRHN, 1988), whereas the mafic–ultramafic rocks in Tongdao and Longsheng areas derived from lithospheric mantle have an area of *c.* 90 km^2 (BGMRGX, 1985). This spatial evolution of the *c.* 760 Ma mafic–ultramafic magmatism in the western Jiangnan orogen resembles that in the Basin and Range Province, in which the mafic magmatism evolved from the sub-alkaline and calc-alkaline series to the OIB-like basaltic rocks, and the magmatic sources accordingly evolved from lithosphere to asthenospheric mantle (Fitton, James & Leeman, 1991; Kempton *et al.* 1991). In particular, the early lithosphere-derived magmas are voluminous, whereas the late asthenosphere-derived OIB-like magmas are relatively less so (< 5 %: Bradshaw, Hawkesworth & Gallagher, 1993; Daley & DePaolo, 1992). The extension of lithosphere accompanied with the upwelling of asthenosphere may be the key factor for the coeval magmas with different sources. According to the model of McKenzie & Bickle (1988), only the lithosphere could be partially melted during the early stage of the extension. However, the contribution of asthenosphere to the generation of mafic magmatism would become ever greater along with the increase in extension of the lithosphere. The geochemical and isotopic characteristics of the *c.* 830–810 Ma arc-like mafic–ultramafic rocks in the Baotan area of northern Guangxi suggest that the lithospheric mantle at the time had been metasomatized by the slab-derived fluids (Zhou, J. C. *et al.* 2004). The upwelling of asthenospheric mantle would immediately follow the break-off and detachment of the subducted oceanic slab (Davies & Blanckenburg, 1995) during the post-orogenic stage, which would at first lead to the extension of overlying metasomatized lithospheric mantle. According to the studies on the sedimentary rocks of the Banxi Group, it has been shown that the Banxi Group was deposited in a littoral–neritic deposition environment at continental margins (Wu, Dai & He, 2001). The depth of the ancient sea might turn deeper from the north to the south (that is, from Guzhang in western Hunan to Longsheng in northern Guangxi) (Tang, Huang & Guo, 1997), which may indicate that the extension in the south would take place earlier than that in the north. The extension

and heating accompanied by the upwelling of the asthenosphere would lead to the partial melting of the metasomatized lithospheric mantle to generate the sub-alkaline mafic rocks in the Tongdao and the Longsheng areas. However, the extension in the Qianyang and Guzhang areas probably took place later and deeper. The small degrees of decompression melting of the deeper asthenospheric mantle would result in the generation of minor alkaline mafic magmas in the area.

The post-orogenic extensional setting revealed by the *c.* 760 Ma mafic rocks of western Hunan supports a normal evolution process of the Jiangnan orogen. It was reported that the Sinian sedimentary sequences conformably overlying these mafic rocks show some features of rifting basin (Liu, Hao & Li, 1999). From this point of view, the formation of the post-orogenic mafic rocks may suggest that the initial rifting in South China might take place after *c.* 760 Ma. This regional rifting that occurred in South China might be a part of the global rifting event of the Rodinia supercontinent. Palaeomagnetic studies on the mafic–ultramafic rocks of western Hunan and comparisons with the published palaeomagnetic data from other areas will shed light on the studies of Rodinia reconstruction in the study area.

8. Conclusions

(1) The Neoproterozoic mafic rocks in western Hunan of South China, the western part of the Jiangnan orogen, yielded ion microprobe U–Pb zircon ages of 747 ± 18 Ma (Qianyang) and 772 ± 11 Ma (Tongdao). They are geochemically divided into two subtypes. The ultramafic rocks from Tongdao are depleted in Nb and Ti and show a decoupled Nd–Hf isotopic signature. Their geochemical features are similar to those of the *c.* 761 Ma sub-alkaline rocks in the Longsheng area of northern Guangxi. However, the alkaline mafic rocks from Qianyang and Guzhang are geochemically similar to OIB and have near-chondritic Nd and Hf isotopic characteristics.

(2) The petrogenesis of two subtypes of the *c.* 760 Ma mafic rocks in western Hunan is different. The ultramafic rocks from Tongdao as well as the mafic–ultramafic rocks from Longsheng in northern Guangxi might be derived from the partial melting of the lithospheric mantle that had been metasomatized during the early oceanic subduction in the area, whereas the mafic rocks from Qianyang and Guzhang might be derived from asthenospheric mantle.

(3) The *c.* 760 Ma mafic magmatism in western Hunan may have been formed in a post-orogenic extensional setting, representing the transition of the tectonic regime from orogenic to anorogenic rifting. The break-off and detachment of the subducted oceanic slab and the accompanied upwelling of the deep asthenospheric mantle might lead to post-orogenic lithospheric extension. The extension might have taken place earlier in the Tongdao and Longsheng areas to generate the relatively great amount of sub-alkaline rocks, whereas the less alkaline mafic rocks in Qianyang and Guzhang might have been generated in the relatively later stage of the extension.

Acknowledgements. This research was financially supported by the National Natural Science Foundation of China (grant nos 40572039 and 40221301), Postgraduate Training Project of Nanjing University and Jiangsu province, China. The manuscript benefited from the comments of the referees, Prof. M. F. Zhou and an anonymous reviewer, and the editors. We also thank Senior Engineers J. Z. Huang, X. S. Tang and J. J. Zheng for their earnest direction and assistance on the field trip, Prof. F. Y. Wu and Dr L. W. Xie for La-MC-ICP-MS zircon Hf isotopic analyses, Prof. F. K. Chen and Dr Z. Y. Chu for Sm-Nd isotopic analysis, Prof. D. Y. Liu for U–Pb zircon analyses, J. F. Gao for trace element analysis, and M. Q. Zhang for major element analysis.

References

ARNDT, N. T. & CHRISTENSEN, U. 1992. The role of lithospheric mantle in continental flood volcanism: thermal and geochemical constraints. *Journal of Geophysical Research* **97**, 10967–81.

BGMRGX (BUREAU OF GEOLOGY AND MINERAL RESOURCES OF GUANGXI PROVINCE). 1985. *Regional Geology of Guangxi Province*. Geological Publishing House, Beijing (in Chinese, with English abstract).

BGMRHN (BUREAU OF GEOLOGY AND MINERAL RESOURCES OF HUNAN PROVINCE). 1988. *Regional Geology of Hunan Province*. Beijing: Geological Publishing House (in Chinese, with English abstract).

BLACK, L. P., KAMO, S. L., WILLIAMS, I. S., MUNDIL, R., DAVIS, D. W., KORSCH, R. J. & FOUDOULIS, C. 2003. The application of SHRIMP to Phanerozoic geochronology: a critical appraisal of four zircon standards. *Chemical Geology* **200**, 171–88.

BLICHERT-TOFT, J., CHAUVEL, C. & ALBAREDE, F. 1997. Separation of Hf and Lu for high-precision isotope analysis of rock samples by magnetic sector-multiple collector ICP–MS. *Contributions to Mineralogy and Petrology* **127**, 248–60.

BONIN, B., SEKKAL, A. A., BUSSY, F. & FERRAG, S. 1998. Alkali-calcic and alkaline post-orogenic (PO) granite magmatism: petrologic constraints and geodynamic settings. *Lithos* **45**, 45–70.

BRADSHAW, T. K., HAWKESWORTH, C. J. & GALLAGHER, K. 1993. Basaltic volcanism in the Southern Basin and Range: No role for a mantle plume. *Earth and Planetary Science Letters* **116**, 45–62.

CHEN, J. F., FOLAND, K. A., XING, F. M., XU, X. & ZHOU, T. X. 1991. Magmatism along the southeast margin of the Yangtze block: Precambrian collision of the Yangtze and Cathysia blocks of China. *Geology* **19**, 815–18.

CHENG, H. 1993. Geochemistry of Proterozoic island-arc volcanic rocks in northwest Zhejiang. *Geochimica* **1**, 18–27 (in Chinese with English abstract).

CLASS, C., ALTHERR, R., VOLKER, F., EBERZ, G. & MCCULLOCH, M. T. 1994. Geochemistry of Pliocene to Quaternary alkali basalts from the Huri Hills, northern Kenya. *Chemical Geology* **113**, 1–22.

COISH, R. A. & SINTON, C. W. 1992. Geochemistry of mafic dikes in the Adirondack mountains: implications for late Proterozoic continental rifting. *Contributions to Mineralogy and Petrology* **110**, 500–14.

COMPSTON, W., WILLIAMS, I. S., KIRSCHVINK, J. L., ZHANG, Z. C. & MA, G. G. 1992. Zircon U–Pb ages for the Early Cambrian time-scale. *Journal of the Geological Society, London* **149**, 171–84.

CVETKOVIĆ, V., PRELEVIĆ, D., DOWNES, H., JOVANOVIĆ, M., VASELLID, O. & PÉCSKAY, Z. 2004. Origin and geodynamic significance of Tertiary postcollisional basaltic magmatism in Serbia (central Balkan Peninsula). *Lithos* **73**, 161–86.

DALEY, E. E. & DEPAOLO, D. J. 1992. Isotopic evidence for lithospheric thinning during extension: Southeastern Great Basin. *Geology* **20**, 104–8.

DAVIES, J. H. & BLANCKENBURG, F. V. 1995. Slab breakoff: A model of lithosphere detachment and its test in the magmatism and deformation of collisional orogens. *Earth and Planetary Science Letters* **129**, 85–102.

DUNPHY, J. M., LUDDEN, J. N. & FRANCIS, D. 1995. Geochemistry of mafic magmas from the Ungava orogen, Québec, Canada, and implications for mantle reservoir compositions at 2.0 Ga. *Chemical Geology* **120**, 361–80.

ENGLAND, P. C. & HOUSEMAN, G. A. 1989. Extension during continental convergence with application to the Tibetan Plateau. *Journal of Geophysical Research* **18**, 1173–7.

FITTON, J. G., JAMES, D., KEMPTON, P. D., ORMEROD, D. S. & LEEMAN, W. P. 1988. The role of lithospheric mantle in the generation of late Cenozoic basic magmas in the western United States. In *Oceanic and continental lithosphere: similarities and differences* (eds K. G. Cox & M. A. Menzies), pp. 331–49. *Journal of Petrology* (Special Lithosphere Issue).

FITTON, J. G., JAMES, D. & LEEMAN, W. P. 1991. Basic magmatism associated with Late Cenozoic extension in the western United States: compositional variation in space and time. *Journal of Geophysical Research* **96**, 13693–711.

FODEN, J., SONG, S. H., TURNER, S., ELBURG, M., SMITH, P. B., VAN DER STELDT, B. & VAN PENGLIS, D. 2002. Geochemical evolution of lithospheric mantle beneath S.E. South Australia. *Chemical Geology* **182**, 663–95.

FRANZINI, M., LEONI, L. & SAITTA, M. 1972. A simple method to evaluate the matrix effect in X-ray fluorescence analysis. *X-ray Spectrometry* **1**, 151–4.

GE, W. C., LI, X. H., LI, Z. X., ZHOU, H. W., WANG, J. & LI, J. Y. 2000. "Longsheng ophiolite" in northern Guangxi revisited. *Acta Petrologica Sinica* **16**, 111–18 (in Chinese with English abstract).

GE, W. C., LI, X. H., LI, Z. X. & ZHOU, H. W. 2001. Mafic intrusions in Longsheng area: age and its geological implications. *Chinese Journal of Geology* **36**, 112–18 (in Chinese with English abstract).

GOOLAERTS, A., MATTIELLI, N., DE JONG, J., WEIS, D. & SCOATES, J. S. 2004. Hf and Lu isotopic reference values for the zircon standard 91500 by MC-ICP-MS. *Chemical Geology* **206**, 1–9.

GUO, L. Z., SHI, Y. S. & MA, R. S. 1980. The geotectonic framework and crustal evolution of South China. In *Scientific paper on geology for international exchange*, pp. 109–16. Beijing: Geological Publishing House (in Chinese with English abstract).

HALLIDAY, A. N., LEE, D. C., TOMMASINI, S., DAVIES, G. R., PASLICK, C. R., FITTON, J. G. & JAMES, D. E. 1995. Incompatible trace elements in OIB and MORB and source enrichment in the sub-oceanic mantle. *Earth and Planetary Science Letters* **133**, 379–95.

HE, A. S. & HAN, X. G. 1992. Characteristics and geological environment of volcanic rocks from Yiyang. *Hunan Geology* **11**, 269–74 (in Chinese with English abstract).

HRGST (HUNAN REGIONAL GEOLOGICAL SURVEY TEAM). 1965. *Regional Geological Survey Report* (Jishou area, 1:200000) (in Chinese).

HRGST (HUNAN REGIONAL GEOLOGICAL SURVEY TEAM). 1999. *Regional Geological Survey Report* (Dasheping area and Qianyang area, 1:50000) (in Chinese).

JIANG, G. Q., SOHL, L. E. & BLICK, N. C. 2003. Neoproterozoic stratigraphic comparison of the Lesser Himalaya (India) and Yangtze block (South China): paleogeographic implications. *Geology* **31**, 917–20.

KELEMEN, P. B., JOHNSON, K. T. M., KINZLER, R. J. & IRVING, A. J. 1990. High-field-strength element depletions in arc basalts due to mantle–magma interaction. *Nature* **345**, 521–4.

KEMPTON, P. D., FITTON, J. G., HAWKESWORTH, C. J. & ORMEROD, D. S. 1991. Isotopic and trace element constraints on the composition and evolution of the lithosphere beneath the southeastern United States. *Journal of Geophysical Research* **96**, 13713–35.

LASSITER, J. C., BLICHERT-TOFT, J., HAURI, E. H. & BARSCZUS, H. G. 2003. Isotope and trace element variations in lavas from Raivavae and Rapa, Cook–Austral islands: constraints on the nature of HIMU- and EM-mantle and the origin of mid-plate volcanism in French Polynesia. *Chemical Geology* **202**, 115–38.

LI, X. H., ZHOU, G. Q., ZHAO, J. X., FANNING, C. M. & COMPSTON, W. 1994. SHRIMP Ion Microprobe Zircon U–Pb Age and Sm–Nd Isotopic Characteristics of the NE Jiangxi Ophiolite and Its Tectonic Implications. *Chinese Journal of Geochemistry* **13**, 317–25.

LI, Z. X., LI, X. H., KINNY, P. D. & WANG, J. 1999. The breakup of Rodinia: Did it start with a mantle plume beneath South China? *Earth and Planetary Science Letters* **173**, 171–81.

LI, Z. X., LI, X. H., KINNY, P. D., WANG, J., ZHANG, S., ZHOU, H. W. 2003. Geochronology of Neoproterozoic syn-rift magmatism in the Yangtze Craton, South China and correlations with other continents: evidence for a mantle superplume that broke up Rodinia. *Precambrian Research* **122**, 85–109.

LIU, H. Y., HAO, J. & LI, R. J. 1999. *Late-Precambrian stratigraphy and geological evolution in the middle-eastern China*. Beijing: Science Press, 200 pp. (in Chinese).

LUDWIG, K. R. 1999. *Using Isoplot/EX, version 2, A Geochronological toolkit for Microsoft Excel*. Berkeley: Berkeley Geochronological Center Special Publication 1a: 47.

MA, L. F., QIAO, X. F., MIN, L. R., FAN, B. X. & DING, X. Z. 2002. *Chinese geological illustrated handbook*, pp. 245–52. Beijing: Geological Publishing House.

MACDONALD, R., MILLWARD, D., BEDDOE-STEPHENS, B. & LAYBOURN-PARRY, J. 1988. The role of tholeiitic magmatism in English Lake district: evidence from dyke in Eskdale. *Mineralogical Magazine* **52**, 459–72.

MAITRE, R. W. L., BATEMAN, P., DUDEK, A., KELLER, J., LEMEYRE, J, BAS, M. J. L., SABINE, P. A., SCHMID, R., SORENSEN, H., STRECKEISEN, A., WOOLEY, A. R. & ZANETTIN, B. 1989. *A classification of igneous rocks and glossary of terms*. Oxford: Blackwell.

MCDONOUGH, W. F. 1990. Constraints on the composition of the continental lithospheric mantle. *Earth and Planetary Science Letters* **101**, 1–18.

MCKENZIE, D. P. & BICKLE, M. J. 1988. The volume and composition of melt generated by extension of lithosphere. *Journal of Petrology* **29**, 625–79.

MCKENZIE, D. P. & O'NIONS, R. K. 1995. The source regions of Ocean Island Basalts. *Journal of Petrology* **36**, 133–59.

MESCHEDE, M. 1986. A method of discriminating between different types of mid-ocean ridge basalts and continental tholeiites with the Nb–Zr–Y diagram. *Chemical Geology* **56**, 207–18.

PEARCE, J. A. 1982. Trace element characteristic of lavas from destructive plate boundaries. In *Andesites* (ed. R. S. Thorpe), pp. 528–48. New York: Wiley.

PEDERSEN, S. A. S., CRAIG, L. E., UPTON, B. G. J., RÄMÖ, O. T., JEPSEN, H. F. & KALSBEEK, F. 2002. Palaeoproterozoic (1740 Ma) rift-related volcanism in the Hekla Sund region, eastern North Greenland: field occurrence, geochemistry and tectonic setting. *Precambrian Research* **114**, 327–46.

POLAT, A. & MÜNKER, C. 2004. Hf–Nd isotope evidence for contemporaneous subduction processes in the source of late Archean arc lavas from the Superior Province, Canada. *Chemical Geology* **213**, 403–29.

QIU, J. X. & ZENG, G. C. 1987. Mineral chemistry of the low-pressure clinopyroxenes from the Cenozoic basalts of Eastern China and its petrological significance. *Acta Petrologica Sinica* **4**, 1–9 (in Chinese with English abstract).

RAO, J. R., WANG, J. H. & CAO, Y. Z. 1993. Deep structures in Hunan Province. *Hunan Geology* **suppl.** (7), pp. 3–854 (in Chinese).

SAUNDERS, A. D., STOREY, M., KENT, W. R. & NORRY, M. J. 1992. Consequences of plume–lithosphere interactions. In *Magmatism and the causes of continental break-up* (eds B. C. Storey, T. Alabaster & R. J. Pankhurst), pp. 41–60. Geological Society of London, Special Publication no. 68.

SAUNDERS, A. D. & TARNEY, J. 1988. Origin of MORB and chemically depleted mantle reservoirs: trace element constraints. *Journal of Petrology (Special Lithosphere Issue)*, 425–45.

SCHERER, E., MÜNKER, C. & MEZGER, K. 2001. Calibration of the lutetium–hafnium clock. *Science* **293**, 683–7.

SHEN, J., ZHANG, Z.Q. & LIU, D. Y. 1997. Sm–Nd, Rb–Sr, $^{40}Ar/^{39}Ar$, and $^{207}Pb/^{206}Pb$ age of the Douling metamorphic complex from eastern Qinling Orogenic belt. *Earth Science – Journal of China University of Geosciences* **18**, 248–54 (in Chinese with English abstract).

SHU, L. S., ZHOU, G. Q., SHI, Y. S. & YIN, J. 1994. Study of high pressure metamorphic blueschist and its late Proterozoic age in the eastern Jiangnan belt. *Chinese Science Bulletin* **39**, 1200–4.

SUN, S. S. & MCDONOUGH, W. F. 1989. Chemical and isotopic systematics of oceanic basalt: implications for mantle composition and processes. In *Magmatism in the Ocean Basins* (A. D. Saunders & M. J. Norry), pp. 313–45. Geological Society of London, Special Publication no. 42.

TANG, X. S., HUANG, J. Z. & GUO, L. Q. 1997. Hunan Banxi Group and its tectonic environment. *Hunan Geology* **16**, 219–26 (in Chinese with English abstract).

THOMPSON, R. N. & MORRISON, M. A. 1988. Asthenospheric and lower lithospheric mantle contributions to continental extension magmatism: an example from the British Tertiary Province. *Chemical Geology* **68**, 1–15.

TEIXEIRA, W., PINESE, J. P. P., IACUMIN, M., GIRARDI, V. A. V., PICCIRILLO, E. M., ECHEVESTE, H., RIBOT, A., FERNANDEZ, R., RENNE, P. R. & HEAMAN, L. M. 2002. Calc-alkaline and tholeiitic dyke swarms of Tandilia, Rio de la Plata craton, Argentina: U/Pb, Sm/Nd, and Rb/Sr $^{40}Ar/^{39}Ar$ data provide new clues for intraplate rifting shortly after the Trans-Amazonian orogeny. *Precambrian Research* **119**, 329–53.

VERVOORT, J. D., PATCHETT, P. J., SÖDERLUND, U. & BAKER, M. 2004. Isotopic composition of Yb and the determination of Lu concentrations and Lu/Hf ratios by isotopic dilution using MC-ICPMS. *Geochemistry Geophysics Geosystems* **5**(11), Q11002: doi 10.1029/2004GC000721.

VILÀ, M., PIN, C., ENRIQUE, P. & LIESA, M. 2005. Telescoping of three distinct magmatic suites in an orogenic setting: Generation of Hercynian igneous rocks of the Albera Massif (Eastern Pyrenees). *Lithos* **83**, 97–127.

WANG, J. 2000. *Neoproterozoic rifting history of south China: significance to Rodinia breakup*. Geological Publishing House, Beijing (in Chinese)

WANG, J. & LI, Z. X. 2003. History of Neoproterozoic rift basins in South China: implications for Rodinia breakup. *Precambrian Research* **122**, 141–58.

WANG, X. L., ZHOU, J. C., QIU, J. S. & GAO, J. F. 2004a. Comment on 'Neoproterozoic granitoids in South China: crustal melting above a mantle plume at c. 825 Ma?' by Xian-Hua Li et al. (PR **122**, 45–83, 2003). *Precambrian Research* **132**, 401–3.

WANG, X. L., ZHOU, J. C., QIU, J. S. & GAO, J. F. 2004b. Geochemistry of the Meso- to Neoproterozoic basic-acid rocks from Hunan Province, South China: implications for the evolution of the western Jiangnan orogen. *Precambrian Research* **135**, 79–103.

WANG, X. L., ZHOU, J. C., QIU, J. S., ZHANG, W. L., LIU, X. M. & ZHANG, G. L. 2006. LA-ICPMS U–Pb zircon geochronology of the Neoproterozoic igneous rocks from northern Guangxi, South China: implications for petrogenesis and tectonic evolution. *Precambrian Research* **145**, 111–30.

WEAVER, B. L. 1991. The origin of ocean island basalt end-member composition: trace element and isotopic constraints. *Earth and Planetary Science Letters* **104**, 381–97.

WILLIAMS, I. S., BUICK, I. S. & CARTWRIGHT, I. 1996. An extended episode of early Mesoproterozoic metamorphic fluid flow in the Reynolds Range, central Australia. *Journal of Metamorphic Geology* **14**, 29–47.

WINCHESTER, J. A. & FLOYD, P. A. 1977. Geochemical discrimination of different magma series and their differentiation products. *Chemical Geology* **20**, 325–43.

WOODHEAD, J., HERGT, J., SHELLEY, M., EGGINS, S. & KEMP, R. 2004. Zircon Hf-isotope analysis with an excimer laser, depth profiling, ablation of complex geometries, and concomitant age estimation. *Chemical Geology* **209**, 121–35.

WU, F. Y., WILDE, S. A., ZHANG, G. L. & SUN, D. Y. 2004. Geochronology and petrogenesis of the post-orogenic Cu–Ni sulfide-bearing mafic–ultramafic complexes in Jilin Province, NE China. *Journal of Asian Earth Sciences* **23**, 781–97.

WU, R. X., ZHENG, Y. F. & WU, Y. B. 2005. Zircon U–Pb age, element and oxygen isotopic geochemistry of Neoproterozoic granodiorites in South Anhui. *Acta Petrologica Sinica* **21**, 587–606 (in Chinese with English abstract).

WU, X. B., DAI, T. G. & HE, S. X. 2001. The geochemical characteristics of light metasedimentary rock for Gaojian Group and their geological implication in the southwest Hunan. *Acta Petrologica Sinica* **17**, 653–62 (in Chinese with English abstract).

XU, P., WU, F. Y., XIE, L. W. & YANG, Y. H. 2004. Hf isotopic compositions of the standard zircons for U-Pb dating. *Chinese Science Bulletin* **49**, 1642–8.

YANG, Z. Y., SUN, Z. M., YANG, T. S. & PEI, J. L. 2004. A long connection (750–380 Ma) between South China and Australia: paleomagnetic constraints. *Earth and Planetary Science Letters* **220**, 423–34.

ZHAO, G. C. & CAWOOD, P. A. 1999. Tectonothermal evolution of the Mayuan assemblage in the Cathaysia Block: implications for Neoproterozoic collision-related assembly of the South China craton. *American Journal of Science* **299**, 309–39.

ZHENG, J. J., JIA, B. H., LIU, Y. R. & CAO, J. H. 2001. Age, magma source and formation environment of mafic–ultramafic rocks in the Anjiang area, western Hunan. *Regional Geology of China* **20**, 164–9 (in Chinese with English abstract).

ZHOU, J. C., WANG, X. L., QIU, J. S. & GAO, J. F. 2004. Geochemistry of Meso- and Neoproterozoic mafic–ultramafic rocks from northern Guangxi, China: arc or plume magmatism? *Geochemical Journal* **38**, 139–52.

ZHOU, J. C., WANG, X. L. & QIU, J. S. 2005. The characters of magmatism in the western section of the Jiangnan Orogenic belt. *Geological Journal of China University* **11**(4), 527–33 (in Chinese with English abstract).

ZHOU, M. F., YAN, D. P., KENNEDY, A. K., LI, Y. Q. & DING, J. 2002. SHRIMP U–Pb zircon geochronological and geochemical evidence for Neoproterozoic arc-magmatism along the western margin of the Yangtze Block, South China. *Earth and Planetary Science Letters* **196**, 51–67.

ZHOU, M. F., LESHER, C. M., YANG, Z. X., LIA, J. W. & SUN, M. 2004. Geochemistry and petrogenesis of 270 Ma Ni–Cu–(PGE) sulfide-bearing mafic intrusions in the Huangshan district, Eastern Xinjiang, Northwest China: implications for the tectonic evolution of the Central Asian orogenic belt. *Chemical Geology* **209**, 233–57.

ZHOU, X. M. & ZHU, Y. H. 1993. Petrological evidences of Neoproterozoic collision-orogenic and suture belts in southeastern China. In *Lithospheric structures and geological evolution in continent from southeastern China* (ed. J. L. Li), pp. 87–97. Beijing: Metallurgical Industry Press (in Chinese).